Assembly of a large earthquake from a complex fault system: Surface rupture kinematics of the 4 April 2010 El Mayor–Cucapah (Mexico) M_w 7.2 earthquake

John M. Fletcher[1,*], Orlando J. Teran[1], Thomas K. Rockwell[2], Michael E. Oskin[3], Kenneth W. Hudnut[4], Karl J. Mueller[5], Ronald M. Spelz[6], Sinan O. Akciz[7], Eulalia Masana[8], Geoff Faneros[2], Eric J. Fielding[9], Sébastien Leprince[10], Alexander E. Morelan[3], Joann Stock[10], David K. Lynch[4], Austin J. Elliott[3], Peter Gold[3], Jing Liu-Zeng[11], Alejandro González-Ortega[1], Alejandro Hinojosa-Corona[1], and Javier González-García[1]

[1]*Departamento de Geologia, Centro de Investigacion Cientifica y de Educacion Superior de Ensenada, Carretera Tijuana-Ensenada No. 3918, Zona Playitas, Ensenada, Baja California, C.P. 22860, México*

[2]*Department of Geological Sciences, San Diego State University, San Diego, California 92182, USA*

[3]*Department of Earth and Planetary Sciences, University of California Davis, One Shields Avenue, Davis, California 95616-8605, USA*

[4]*U.S. Geological Survey, 525 & 535 S. Wilson Street, Pasadena, California 91106-3212, USA*

[5]*Department of Geological Sciences, University of Colorado Boulder, Boulder, Colorado 80309, USA*

[6]*Universidad Autónoma de Baja California, Facultad de Ciencias Marinas, Carretera Tijuana-Ensenada No. 3917, Zona Playitas, Ensenada, Baja California, C.P. 22860, México*

[7]*Department of Earth, Planetary and Space Sciences, University of California Los Angeles, 595 Charles Young Drive East, Los Angeles, California 90095, USA*

[8]*Departament de Geodinàmica i Geofísica, Universitat de Barcelona, Zona Universitària de Pedralbes, Barcelona 08028, Spain*

[9]*Jet Propulsion Laboratory, California Institute of Technology, M/S 300-233, 4800 Oak Grove Drive, Pasadena, California 91109, USA*

[10]*Division of Geological and Planetary Sciences, California Institute of Technology, Pasadena, California 91125, USA*

[11]*State Key Laboratory of Earthquake Dynamics, Institute of Geology, China Earthquake Administration, A1# Huayanli, Dewai Avenue, Chaoyang District, P.O. Box 9803, Beijing 100029, China*

ABSTRACT

The 4 April 2010 moment magnitude (M_w) 7.2 El Mayor–Cucapah earthquake revealed the existence of a previously unidentified fault system in Mexico that extends ~120 km from the northern tip of the Gulf of California to the U.S.–Mexico border. The system strikes northwest and is composed of at least seven major faults linked by numerous smaller faults, making this one of the most complex surface ruptures ever documented along the Pacific–North America plate boundary. Rupture propagated bilaterally through three distinct kinematic and geomorphic domains. Southeast of the epicenter, a broad region of distributed fracturing, liquefaction, and discontinuous fault rupture was controlled by a buried, southwest-dipping, dextral-normal fault system that extends ~53 km across the southern Colorado River delta. Northwest of the epicenter, the sense of vertical slip reverses as rupture propagated through multiple strands of an imbricate stack of east-dipping dextral-normal faults that extend ~55 km through the Sierra Cucapah. However, some coseismic slip (10–30 cm) was partitioned onto the west-dipping Laguna Salada fault, which extends parallel to the main rupture and defines the western margin of the Sierra Cucapah. In the northernmost domain, rupture terminates on a series of several north-northeast–striking cross-faults with minor offset (<8 cm) that cut uplifted and folded sediments of the northern Colorado River delta in the Yuha Desert.

In the Sierra Cucapah, primary rupture occurred on four major faults separated by one fault branch and two accommodation zones. The accommodation zones are distributed in a left-stepping en echelon geometry, such that rupture passed systematically to structurally lower faults. The structurally lowest fault that ruptured in this event is inclined as shallowly as ~20°. Net surface offsets in the Sierra Cucapah average ~200 cm, with some reaching 300–400 cm, and rupture kinematics vary greatly along strike. Nonetheless, instantaneous extension directions are consistently oriented ~085° and the dominant slip direction is ~310°, which is slightly (~10°) more westerly than the expected azimuth of relative plate motion, but considerably more oblique to other nearby historical ruptures such as the 1992 Landers earthquake. Complex multifault ruptures are common in the central portion of the Pacific North American plate margin, which is affected by restraining bend tectonics, gravitational potential energy gradients, and the inherently three-dimensional strain of the transtensional and transpressional shear regimes that operate in this region.

INTRODUCTION

Large surface ruptures that cascade slip along multiple faults offer an opportunity to learn about mechanical relationships between faults, along with factors that control the state

*Corresponding author: jfletche@cicese.mx

Geosphere; August 2014; v. 10; no. 4; doi:10.1130/GES00933.1; 25 figures; 6 supplemental files.
Received 25 March 2013 ♦ Revision received 18 March 2014 ♦ Accepted 25 April 2014

of stress in the seismogenic crust. The 4 April 2010, moment magnitude (M_w) 7.2 El Mayor–Cucapah (EMC) earthquake activated slip on at least 7 different faults; many were unnamed and some were not even known to exist prior to the earthquake. Most of the faults have relatively short total strike lengths (<30 km), none of them control topography, and Holocene paleoscarps are rare. Individually each fault could have been thought to present a low seismic risk, and no one suspected that they had the physical links required for them to behave as a single fault system that was capable of producing a major earthquake. The fault system has strands that dip at very shallow angles (as low as 20°) and are likely to be severely misoriented relative to the inferred regional stress. Along its entire length, the complex fault system is located within 1–3 km of faults that can be considered the dominant strands of the plate margin in this area. These dominant faults include the Laguna Salada and Cerro Prieto faults, which have produced many major historical earthquakes and together accommodate to 90% of relative plate motion (Anderson and Bodin, 1987; Mueller and Rockwell, 1991; Bennett et al., 1996; Genrich et al., 1997). Therefore, the EMC rupture significantly tests our understanding of rock mechanics and failure criteria to explain why plate-margin shearing bypassed optimally oriented faults to become partitioned onto an adjacent complex fault network.

The EMC surface rupture is arguably the most complex ever documented on the Pacific–North American plate margin (Fig. 1). However, multifault ruptures that have complex kinematics and occur off of the main strands of the plate margin are not uncommon in the central portion of the plate margin, as is well demonstrated by the three most recent earthquakes in this region, including the M 7.2 EMC in 2010, M 7.1 Hector Mine in 1999, and M 7.3 Landers in 1992 (Fig. 2). We argue that the central domain of the plate margin is affected by several geodynamic processes, including regional redistribution of plate margin shearing, gravitational potential energy gradients emanating from the Great Basin, and the inherently three-dimensional strain of transtensional and transpressional shearing. We propose that these factors help explain the surprising and somewhat unpredictable nature of major earthquakes as well as the complex fault behavior observed throughout the central domain of the plate boundary.

In this paper we present field offset measurements, field and lidar (light detection and ranging) derived mapping, and kinematic analysis of the 2010 EMC surface rupture. We provide further insight into the deep complexity beneath the superficial simplicity of the rupture, which, when viewed from the far field (S. Wei et al., 2011), belies a complex array of faults, at places spread across a zone >3 km in width, that slipped together in this earthquake. North of the epicenter, within the Sierra Cucapah, excellent exposures of the surface rupture through bedrock and coarse alluvial sediments provide a wealth of slip data from which to infer how this fault system assembled to generate a major earthquake. We find that despite the great complexity of the surface rupture and its kinematic behavior, the overall strain released by this earthquake was consistent with interseismic deformation, which deviates slightly from expected plate motion, but is considerably oblique to other nearby historical ruptures such as the 1992 Landers earthquake. The overall consistency of strain, despite the variety of faulting involved, could indicate that fault rupture was guided overall by a relatively smooth pre-earthquake stress field.

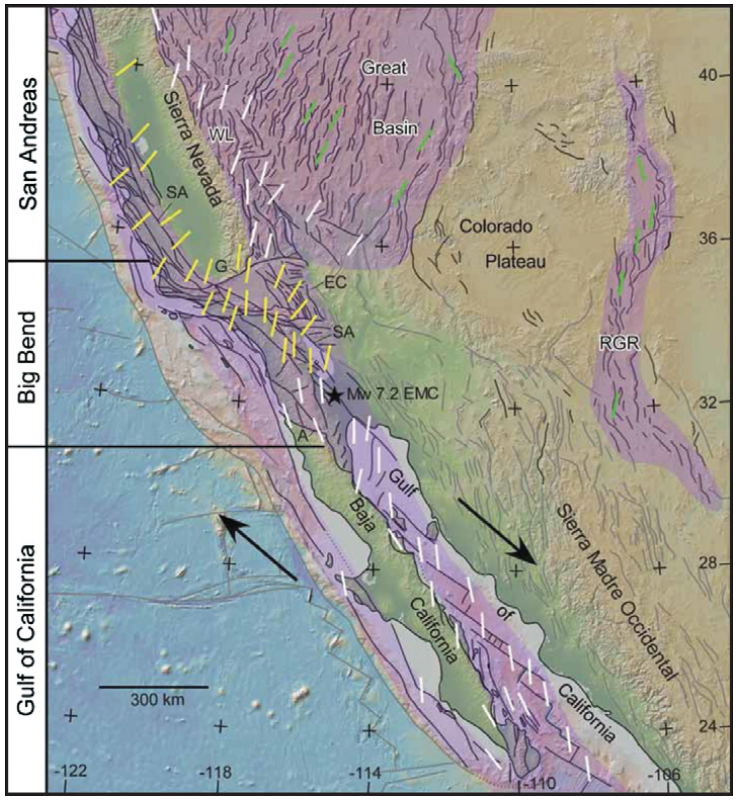

Figure 1. Tectonic map of western North America showing the main shear zones (purple shading) that compose the Pacific North American plate margin. Simplified fault traces include Quaternary faults (black; simplified from U.S. Geological Survey, 2006; and regional mapping in western Mexico by us, i.e., Fletcher and others) and inactive Neogene faults (gray; simplified from Muehlberger, 1996). Maximum horizontal compressive stress shown by thick horizontal lines defines regions of transtension (white), transpression (yellow), and extension (green) (simplified from World Stress Map database; Heidbach et al., 2008). In this study the plate margin is divided into three main domains: Gulf of California, Big Bend, and San Andreas. Transtensive relative plate motion is accommodated in a narrow belt in the Gulf of California with minor slip (~5 mm/yr) occurring in the continental shelf west of Baja California (Dixon et al., 2000). In the Big Bend domain, plate margin shearing changes from transtensive to transpressive and bifurcates into the north-northwest–trending eastern California shear zone (EC) and a network of west-northwest–striking faults that includes the Big Bend segment of the San Andreas fault. In the San Andreas domain, relative plate motion is partitioned into the transpressive San Andreas fault system (SA), transtensive Walker lane shear zone (WL), and extension in the Great Basin. Minor extension is also partitioned into the Rio Grande Rift (RGR), which forms an isolated belt of shearing that overlaps with portions of all three domains. Black star marks epicenter of the 4 April 2010 M_w 7.2 El Mayor–Cucapah earthquake located within the Big Bend domain. A—Agua Blanca fault, G—Garlock fault.

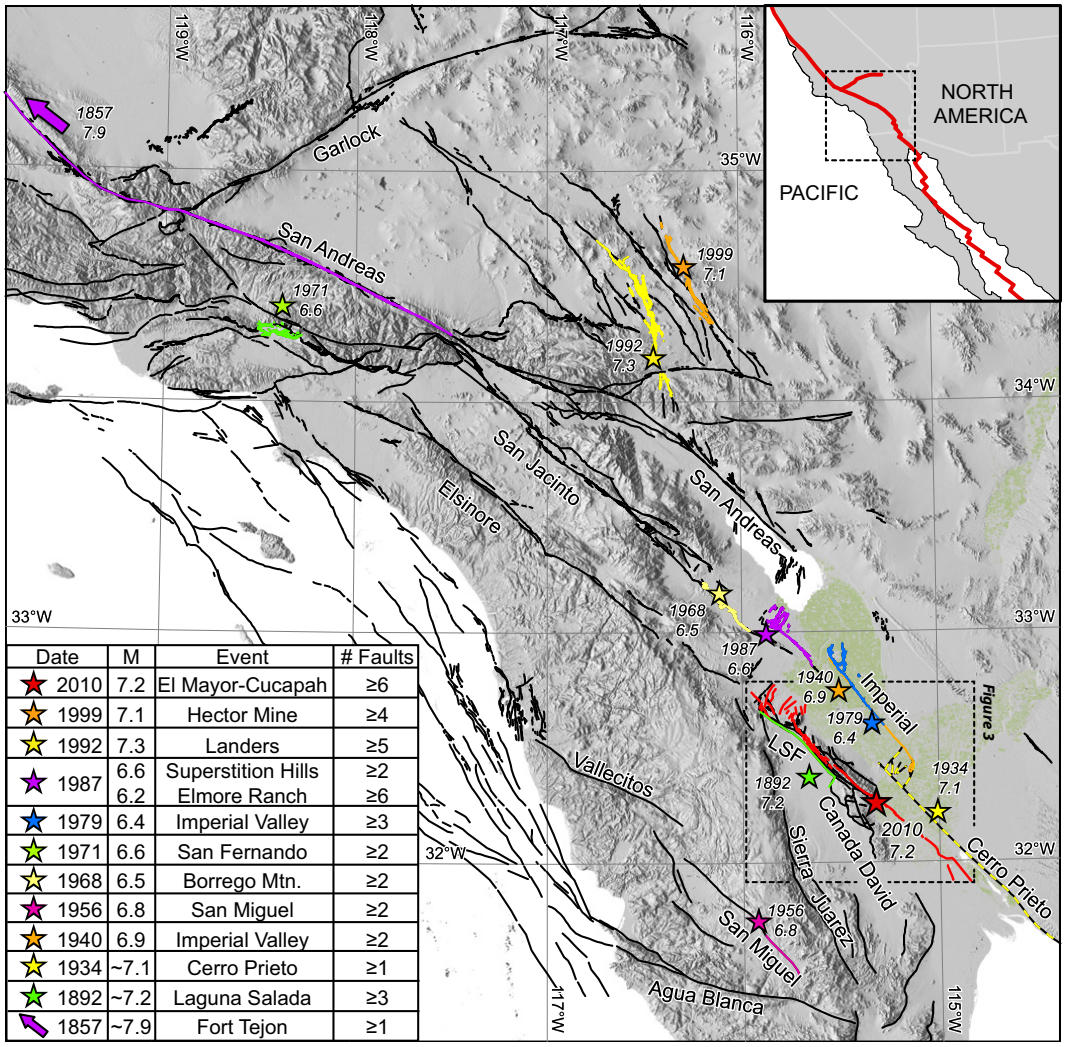

Date	M	Event	# Faults
2010	7.2	El Mayor-Cucapah	≥6
1999	7.1	Hector Mine	≥4
1992	7.3	Landers	≥5
1987	6.6 6.2	Superstition Hills Elmore Ranch	≥2 ≥6
1979	6.4	Imperial Valley	≥3
1971	6.6	San Fernando	≥2
1968	6.5	Borrego Mtn.	≥2
1956	6.8	San Miguel	≥2
1940	6.9	Imperial Valley	≥2
1934	~7.1	Cerro Prieto	≥1
1892	~7.2	Laguna Salada	≥3
1857	~7.9	Fort Tejon	≥1

Figure 2. Tectonic map of the Big Bend domain or the central domain of the Pacific North American plate margin showing simplified fault traces (black) and historic ruptures (colored). Fault traces north of the international border are from the U.S. Geological Survey (2006) Quaternary fault and fold database. Most historic ruptures have activated multiple faults and are located off the main plate margin fault system composed of the San Andreas, Imperial, and Cerro Prieto faults (bold red line on the inset map). The 2010 El Mayor–Cucapah (EMC) earthquake activated slip on a minimum of 6 discrete faults, and inset table shows that on this basis alone it is arguably the most complex of all historic ruptures in the region. LSF—Laguna Salada fault.

SEISMOTECTONIC SETTING

The 2010 M_w 7.2 EMC earthquake is located in the central portion of the Pacific–North American plate margin, which contains the Big Bend segment of the San Andreas fault. The Big Bend is the prominent left-stepping restraining bend in the southern San Andreas fault (Hill and Dibblee, 1953) and is known to rupture in great earthquakes due to elevated normal stress (Sykes and Seeber, 1985). Faulds and Henry (2008) proposed that the Big Bend of the San Andreas formed due to the linking of plate margin shearing in the Gulf of California with the older portion of the San Andreas system established along the California coast. Although the timing of the onset of transtensional plate margin shearing in the Gulf of California is controversial, it can be no younger than 5.5 Ma (Oskin and Stock, 2003) and may be as old as 12.5 Ma (Fletcher et al., 2007). Regardless of the timing of its initiation, the southern San Andreas fault is not the only fault that has transected the mechanically competent Cretaceous batholith that exists as a continuous belt along the entire length of the plate margin. Rather, a complex network of faults as far south as the Agua Blanca fault operate together to accommodate strain compatibility between the two offset and kinematically distinct domains of plate margin shearing (Figs. 1 and 2). However, only ~80% of the total relative plate motion is transferred to coastal California (Freymueller et al., 1999; Argus and Gordon, 2001) through this left-stepping network, and other fault systems in the central domain such as the eastern California shear zone and the Garlock fault transfer plate margin shearing throughout the Great Basin from the Walker Lane belt to the Wasatch front. In this study we define the central domain of plate margin shearing to include all faults that accommodate the redistribution of plate margin shearing from the narrow integrated transtensional fault network in the Gulf of California to the more regionally distributed and kinematically partitioned systems in the north. This central domain is here named the Big Bend domain and extends from the Garlock fault in the north to the Agua Blanca fault in the south (Fig. 2). We submit that the redistribution of plate margin shearing is only one of several geodynamic processes that combine to produce complex multifault ruptures like the EMC earthquake.

The EMC earthquake occurred in the southernmost portion of the Big Bend domain and represents the largest seismic moment release at this latitude of the Pacific–North American plate margin since 1892 (Fig. 2). The primary surface rupture and seismicity are distributed along a complex fault network that extends ~120 km along an azimuth of 315° from the northern tip of the Gulf of California to the U.S.-Mexico border, which makes it the longest historical surface rupture for this domain. Triggered slip was observed on most faults in the immediate vicinity of the EMC rupture sequence, as well as on

significant portions of active faults as far north as the Mecca Hills segment of the San Andreas fault, more than 160 km away from the epicenter (Rymer et al., 2011; M. Wei et al., 2011).

In the immediate vicinity of the 2010 rupture, two major fault systems have been recognized that control topography and are thought to accommodate most of the plate margin shearing at this latitude: the Imperial–Cerro Prieto fault to the east, and the Laguna Salada–Cañada David fault system (Fig. 3; e.g., Mueller and Rockwell, 1991; Bennett et al., 1996; Genrich et al., 1997; Axen and Fletcher, 1998) to the west. Both of these fault systems exhibit Holocene scarps and have generated at least three historical earthquakes that were similar in magnitude to the 2010 earthquake (Fig. 3; Anderson and Bodin, 1987; Mueller and Rockwell, 1991; Hough and Elliot, 2004). The Imperial and Cerro Prieto faults are located along the axis of the Mexicali basin and can be considered the dominant faults of the plate boundary at this latitude (Fig. 3). These two faults have linear traces, and are oriented with an azimuth of 315° ± 5°. Earthquake focal mechanisms and surface ruptures indicate that they accommodate strike slip and likely represent nascent transform faults (Faulds and Henry, 2008). Like other major transform faults in the Gulf of California, the Imperial and Cerro Prieto faults have an en echelon geometry and significant modern volcanic activity. The world's second largest geothermal field is located at Cerro Prieto, where the two faults meet at an extensional stepover (Lira-Herrera, 2005). Modeling of global positioning system (GPS) geodetic data indicate 42 ± 1 mm/yr of slip on this fault system, which is ~87% of the total between the Pacific and North America plates (Bennett et al., 1996; Genrich et al., 1997).

The Laguna Salada fault and Cañada David detachment fault, located to the west of the 2010 surface rupture, compose another important active fault system that controls subsidence of the Laguna Salada basin and uplift of the Sierra Cucapah and Sierra El Mayor (Fig. 3; Axen and Fletcher, 1998; Fletcher and Spelz, 2009). The Cañada David detachment is an active low-angle normal fault with west-directed (hanging wall moves west) tectonic transport. The Laguna Salada fault dips steeply to the west, accommodates oblique dextral-normal slip (Mueller and Rockwell, 1995), and essentially acts as an oblique ramp for the detachment (Fletcher and Spelz, 2009). Geologic and geodetic studies indicate that this two-fault system accommodates 2–4 mm/yr of displacement (Savage et al., 1994; Mueller and Rockwell, 1995). Therefore, together the Laguna Salada–Cañada David and Cerro Prieto–Imperial fault systems accommo-

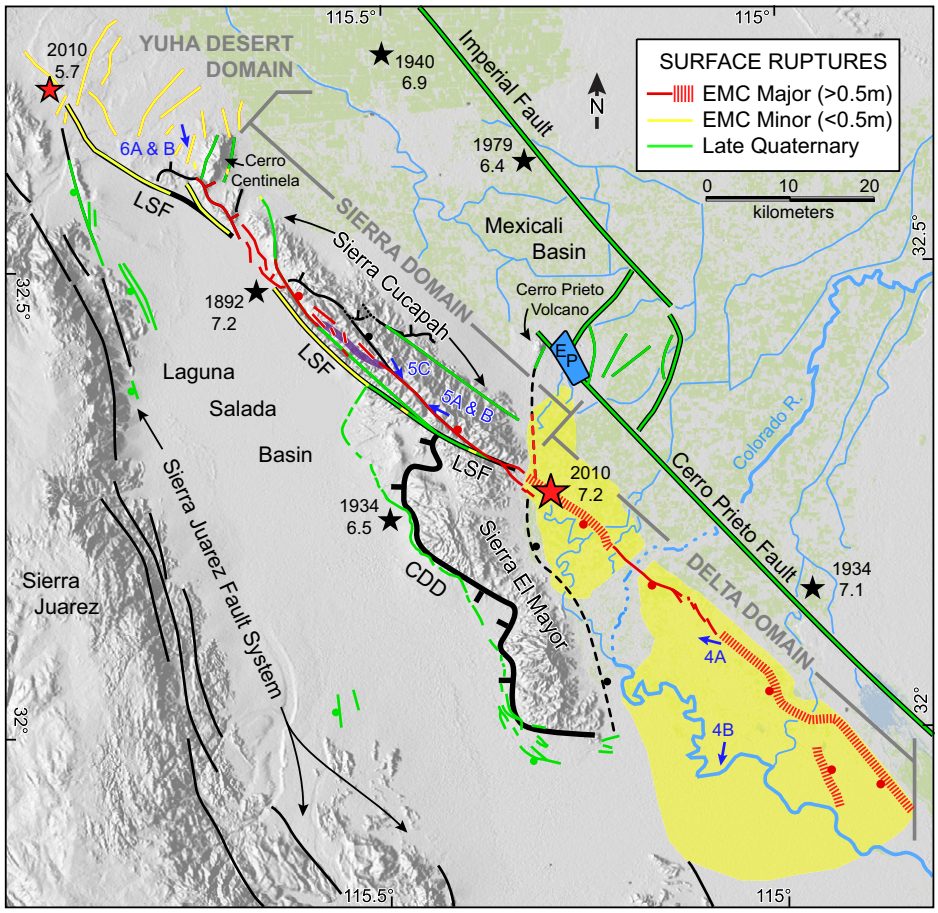

Figure 3. Map showing the main shock epicenter of El Mayor–Cucapah (EMC) (red star), progenitor fault of this earthquake sequence (red dotted line north of epicenter), and three macroscopic domains of the surface rupture, which include Yuha Desert, Sierra, and Delta domains. The EMC rupture activated slip on seven different faults that exist between two dominant faults systems (thick line traces) that control topography and accommodate most plate margin shearing (e.g., Mueller and Rockwell, 1991; Bennett et al., 1996; Genrich et al., 1997; Axen and Fletcher, 1998). These include the Cerro Prieto–Imperial system and the Laguna Salada (LSF)–Cañada David (CDD) fault system. The yellow shaded envelopes in the Delta domain demarcate the approximate limits of distributed liquefaction and surface failure, which was absent along the intermittent section of the Colorado River (blue line with three-dot ornamentation; currently dry and does not display ground failure). In the Delta domain, laterally continuous coseismic surface displacements were only observed by remote sensing methods including synthetic aperture radar interferometry (thick red hachures) and pre-event and post-event lidar (light detection and ranging) elevation differences (solid red lines). Also shown are epicenter locations of historical earthquakes (black stars; downloaded from Southern California Seismic Network earthquake catalog; Hutton et al., 2010) and older rupture traces (green lines; Sharp et al., 1982; Anderson and Bodin, 1987; Axen et al., 1999; Suarez-Vidal et al., 2007). Late Pleistocene ruptures are also found on faults with historical ruptures; not all known late Pleistocene ruptures are shown. Blue arrows mark locations of photos shown in Figures 4–6. Green patterns in the base map show active farmlands in the Imperial and Mexicali Valleys. Shaded relief map is produced from Shuttle Radar Topography Mission data. EP is the evaporation pond of the Cerro Prieto geothermal field. Purple line in Sierra domain delineates a gradient in surface displacement detected by COSI-Corr (co-registration of optically sensed images and correlation) pixel tracking; see text section on Puerta accommodation zone for more details.

date more than ~90% of the full plate motion budget. The remaining slip is most likely to be accommodated by three other fault zones west of Laguna Salada: the Sierra Juarez normal fault, and the San Miguel–Vallecitos and Agua Blanca faults (Fig. 2), both of which are predominantly dextral strike-slip faults.

Perhaps the biggest surprise of the EMC earthquake is that it did not rupture any of the four well-known active fault systems at this latitude (Imperial, Cerro Prieto, Laguna Salada, Cañada David), but rather occurred on an obscure and, in part, unrecognized system of faults. Very few of these faults control topography, and slip in 2010 actually lowered much of the range crest of the Sierra Cucapah, which suggests that the fault system has had a much lower slip rate than the adjacent major faults. Likewise, faulting in the Colorado River delta occurred along a buried fault that failed to propagate to the surface as a discrete fault scarp due to the transfer of coseismic slip to more penetrative strain distributed throughout the thick sequence of water-saturated deltaic sediments (Oskin et al., 2012), as has been proposed for a similar rupture style in the New Madrid area (Missouri, United States; e.g., Guccione et al., 2000).

OVERVIEW OF THE 2010 SURFACE RUPTURE

The epicenter of the 2010 EMC earthquake is located near the center of its rupture zone, and coincides with the boundary between two distinct kinematic faulting domains that have profoundly contrasting geomorphologic expressions (Fig. 3). To the south of the epicenter, the rupture cuts across the plain of the Colorado River delta and is herein named the Delta domain (Fig. 3). North of the epicenter, rupture follows an east-dipping stack of oblique-slip faults through the high portions of the Sierra Cucapah, which we refer to as the Sierra domain. Both domains accommodate dextral displacement. However, south of the epicenter the dominant vertical sense of offset is down to the southwest, whereas north of the epicenter the dominant sense of vertical slip is down to the northeast. Near the lateral limits of the rupture, fractures have a more northerly strike and show macroscopic right-stepping curvatures relative to the strike of the main rupture. The northern limit of the rupture is dominated by north-northeast–striking cross-faults, similar to those that rupture in the 1987 Superstition Hills earthquake sequence (Hudnut et al., 1989) but on a scale at least 10 times larger in area; this zone composes a third kinematic domain, which we call the Yuha Desert domain (Fig. 3). Here we describe the overarching characteristics of rupture in each domain, as well as relevant aspects of its geology. This is followed by a more detailed examination of the faulting in the Sierra Cucapah, where most field observations were obtained.

Delta Domain

Vast fields of liquefaction and fracturing distributed across an area of ~833 km^2 are the dominant expression of the EMC coseismic surface failure in the Delta domain (Fig. 3). The Colorado River delta has very low relief and an average elevation close to sea level. Most of this area is actively subsiding beneath a cover of late Holocene sediment that caps a thick sequence of late Neogene deltaic deposits. Sedimentary backfilling of fault-controlled basins like that in the Cerro Prieto stepover exceeds 5 km in thickness (Dorsey, 2010). Despite fast slip rates and the focusing of plate margin shearing on faults in this domain, the surface expression of faulting is not well defined (e.g., Biehler et al., 1964; Suarez et al., 1982). For example, the M 7.1 1934 Cerro Prieto and M 6.1 1980 Victoria earthquakes on the Cerro Prieto fault produced extensive liquefaction throughout the region, but geologists associated with later field surveys could not identify scarps with appreciable tectonic displacement and no continuous surface rupture was observed (Biehler et al., 1964; Suarez et al., 1982). Although it is clear that the EMC rupture did not occur on any of the main faults in the Delta domain (i.e., Imperial–Cerro Prieto faults), its surface expression is in many ways similar to that of previous events.

Despite the vast size of the zone of surface failure in the Delta domain, individual fractures have relatively short strike lengths, typically hundreds of meters, and they vary widely in orientation. Coseismic fracture arrays are commonly marked by extensive sand blows and subparallel anastomosing arrays of tectonic scarps are typically intersected by other sets of fractures (Fig. 4A). Many sand-blow fracture arrays have strongly curvilinear traces that show progressive changes in strike of more than 180°. Such arrays appear to be associated with shallowly buried sand bars deposited along meanders in ancient river systems (Fig. 4). Therefore, a significant proportion of fracture sets likely formed by dewatering of buried sediments due to vigorous coseismic shaking, and need not accommodate tectonic displacements or be located in close proximity to a buried fault with coseismic rupture. Curving zones of liquefaction and fracturing have also been associated with head scarps of lateral spreads, such as those associated with the New Madrid earthquake sequence (e.g., Penick, 1976). Nonetheless, some scarps have as much as 1 m of vertical offset and many arrays are arranged in an en echelon configuration. The sense of stepping in the en echelon arrays indicates a component of lateral shear that changes systematically with orientation. In general, northwest-striking en echelon arrays are more abundant and show a left-stepping geometry with dextral lateral offset, whereas north-northeast–striking en echelon arrays are right stepping and record sinistral lateral offset. These kinematics are consistent with north-south shortening and east-west extension, which is typical of the general kinematics of plate margin shearing in this area.

Two macroscopic fields of intense liquefaction have been identified from aerial surveys conducted within months of the EMC earthquake as well as Google Earth imagery generated over a period of two years after the earthquake (Figs. 3 and 4). In general, fractures and sand blows are much more common near perennial stream channels and the most active agricultural fields, which were likely to have been more heavily irrigated prior to the EMC rupture. It is interesting that the fields of liquefaction and fracturing do not cross the modern channel of the Colorado River. Although paleo–sand blows and paleo–mud volcanoes are observed in pre-2010 Google Earth satellite imagery, such features associated with the EMC earthquake are absent. Another feature that is absent from the main channel of the Colorado River in this area is perennial water flow, due its upstream diversion through a network of canals to other portions of the delta (Fig. 3). The region surrounding the main channel likely underwent the same amount of vigorous shaking as the adjacent areas with extensive liquefaction and fracturing. Therefore the lack of water-saturated sediments at sufficiently shallow levels in the subsurface is the most likely reason for the absence of ground failure, and the main channel, which used to be the wettest part of the delta during previous large earthquakes, is now the driest.

As was the case with the previous two large earthquakes in the southern Colorado River delta (Kovach et al., 1962; Biehler et al., 1964; Suarez et al., 1982), geologists working on the EMC earthquake through field surveys and conventional photographic imagery alone would not be able to recognize laterally continuous surface rupture controlled by discrete faults at depth. Nonetheless, a systematic sense of dextral west-down surface displacement (50–300 cm) was detected with synthetic aperture radar (SAR) interferometry and pixel offset tracking analysis of ALOS PALSAR (Advanced Land Observing Satellite, Phased Array L-band SAR; EORC—Earth Observation Research Center, JAXA—Japan Aerospace Exploration Agency) imagery

Figure 4. Oblique aerial photos of El Mayor–Cucapah (EMC) rupture in the Delta domain (photo locations plotted in Fig. 3). (A) Northwest-striking tectonic scarps (yellow arrows) cut across abandoned and buried meanders (red dashed lines) of the Colorado River delta. White deposits are coseismic sand blows that erupted along tectonic fractures and buried sandbars. Photo azimuth is ~285°. (B) White deposits generated by dewatering and liquefaction are observed throughout the southern Colorado River delta and extend to the margin of the Sierra Pinta (red arrows), which is more than 12 km from the main zone of tectonic surface rupture (Fig. 3). Prominent fractures along the axis of the elongated sand blow deposits curve and follow abandoned and buried meanders (red dashed lines). Photo azimuth is ~190°. Photos taken by John M. Fletcher. See Supplemental Files 1 and 2 (see footnotes 1 and 2) for photo information in Google Earth KMZ format and Microsoft Excel table format, respectively.

along a continuous trace that extends ~55 km to the southeast of the main shock epicenter (Fig. 3; S. Wei et al., 2011). Slip on the main faults probably does not reach the surface in the thick sediments of the Colorado delta. Waveform modeling and SAR pixel offsets suggest a relatively simple subsurface fault geometry in this region with coseismic rupture controlled by a single west-dipping master fault, the Indiviso fault (S. Wei et al., 2011). However, significant fault strands with an east-down component of coseismic slip and postseismic slip were also detected with ALOS PALSAR interferometry in the southern delta region (Nelson et al., 2013), and seismic reflection profiles across the southern delta demonstrate the existence of a major transtensional basin to the west of the Cerro Prieto fault, which is controlled by a family of west-dipping faults that sole into an east-dipping detachment (Chanes-Martinez, 2012). This kinematically and geometrically complex system of newly discovered faults underlies the vast region of coseismic surface failure in the southern Colorado River delta (Fig. 3).

Pre-event and post-event lidar surveys provided a way to directly calculate the coseismic changes in surface elevation and revealed displacements of as much as 50 cm in the vertical component across buried faults that could be traced laterally for 12 km (Oskin et al., 2012). In Oskin et al. (2012), the surface rupture in the delta was described as having an unusual style where kilometer-length, discontinuous curvilinear shear zones are associated with gentle, 100-m-wide ramps, across which the topography steps by ~50 cm in elevation. The traces of these surface displacements coincide very well with the central segment of the ALOS PALSAR derived trace, but lidar provided even more detail into the geometric complexity and branching of faults at depth (Fig. 3). Fault splays typically have a left-stepping en echelon configuration and strike more northerly than the overall trace of the surface rupture, which suggests that they likely accommodate the dextral component of coseismic displacement (Fig. 3).

The fields of intense liquefaction do not symmetrically surround the lidar and SAR based traces of surface displacement, but instead are largely located in the downthrown block to the southwest (Fig. 3). This relationship is especially well displayed with the larger, southern field of liquefaction (Fig. 3). A seismic refraction profile collected recently as part of the Salton Seismic Imaging Project is located near the main shock epicenter and demonstrates the existence of a major fault in the subsurface that dips 50° to the southwest and projects toward the lidar and SAR based traces of surface displacement along the northeastern limit of intense surface fracturing and liquefaction (Ramirez-Ramos, 2013). Several studies have reported that stronger ground motions occur in the hanging wall than in the footwall of dipping faults (e.g., Abrahamson and Somerville, 1996; Oglesby et al., 1998), regardless of kinematics (Oglesby et al., 2000). The larger ground motions in the hanging-wall block arise from the trapping of seismic waves between the ground surface and the master fault (Oglesby et al., 1998, 2000; Ma and Beroza, 2008). Therefore, the distribution of ground failure in the Delta domain is not only controlled by the extent of fluid-saturated cohesionless sediments, but also by the southwest-dipping orientation of the buried master fault.

The northern field of liquefaction deviates significantly from the trace of the SAR based surface displacement and projects much farther to the north along the edge of the southern Sierra Cucapah, which suggests that it was at least partially controlled by rupture on a different fault (Fig. 3). A separate branch of surface displacement near the main-shock epicenter has yet been identified by remote sensing, but the north-trending salient in the field of intense liquefaction corresponds very well with a similar salient in the distribution of the EMC aftershock series (Hauksson et al., 2010). Based on wave-form modeling, S. Wei et al. (2011) proposed that EMC rupture initiated on a north-striking fault near the epicenter as an M_w 6.3 subevent with normal dip slip and later became transferred to the northwest-striking faults that control the main surface rupture in the Delta and Sierra domains. Armstrong et al. (2010) documented significant Quaternary uplift and proposed the existence of a major range-bounding normal fault along the eastern mountain front of Sierra El Mayor and southeast end of Sierra Cucapah. The northern segment of this east-dipping fault is likely to be the progenitor normal fault that initiated the EMC earthquake. Its surface trace most likely coincides with the western margin of the northern field of intense liquefaction, which projects toward late Pleistocene fault scarps along the southwestern side of Cerro Prieto (Fig. 3). If true, the distribution of liquefaction in the northern field also largely occurs in the hanging wall of a major fault system that accommodated coseismic rupture at depth.

In summary, several processes controlled the formation of fracture arrays in the Delta domain, including (1) tectonic slip on buried faults, (2) hydrofracturing associated with liquefaction of material in buried sand bars of the Colorado River delta, and (3) gravitational collapse along the margins of river channels, irrigation canals, and other linear topographic features. Fractures formed by the latter two processes are produced by severe shaking, and thus all three mechanisms are related ultimately to seismogenic slip on tectonic faults at depth. In this study we document the existence of at least three rupture-controlling faults in the Delta domain. The diffuse nature of surface fracturing and incomplete coverage of imagery taken immediately after the 2010 earthquake has inhibited a more systematic structural analysis of the rupture in this domain.

Sierra Domain

Most of the northern half of the main rupture is called the Sierra domain. Here the rupture propagated 55 km through an imbricate stack of east-dipping faults along the western slope of the Sierra Cucapah (Fig. 3). In contrast to the Delta domain, where only late Quaternary sediments occur at the surface, the Sierra domain exposes pre-Cenozoic crystalline rocks as well as Miocene and younger volcanic and sedimentary strata, forming a very high relief mountain range reaching more than 1000 m in elevation. Although much of the surface rupture occurred in remote mountainous regions, it is very well exposed with a plethora of offset geomorphic features. Therefore, it is in this domain where we focused the most comprehensive structural analysis and detailed mapping to characterize the geometry and kinematics of faulting, which is presented in detail in the following sections.

An overarching characteristic of the rupture in the Sierra domain is its structural complexity at the surface. The surface rupture has breaks along multiple fault strands, and kinematics are dominated by oblique dextral-normal slip with an overall east-down sense of shear, which lowered the high topography of the Sierra Cucapah (Fig. 5). As distance from the epicenter increases toward the north, rupture passes systematically to structurally lower strands in the imbricate fault stack. Structurally lower fault strands in the stack have systematically shallower dips and the structurally lowest Paso Superior fault is inclined at angles as low as 20°. Part of the complexity of the rupture can be attributed to interaction with oblique-slip detachment faults that caused the rupture to branch into numerous strands within a few kilometers of the surface.

Yuha Desert Domain

In the Yuha Desert domain, surface rupture returns to the low-relief Colorado River delta, which is both structurally and geomorphologically distinct from the Sierra domain (Fig. 3). Faults in the Yuha Desert domain generally have a much more northerly orientation than those in the Sierra domain, and many strike northeast, nearly orthogonal to the strike of the primary rupture farther south. Surface rupture is com-

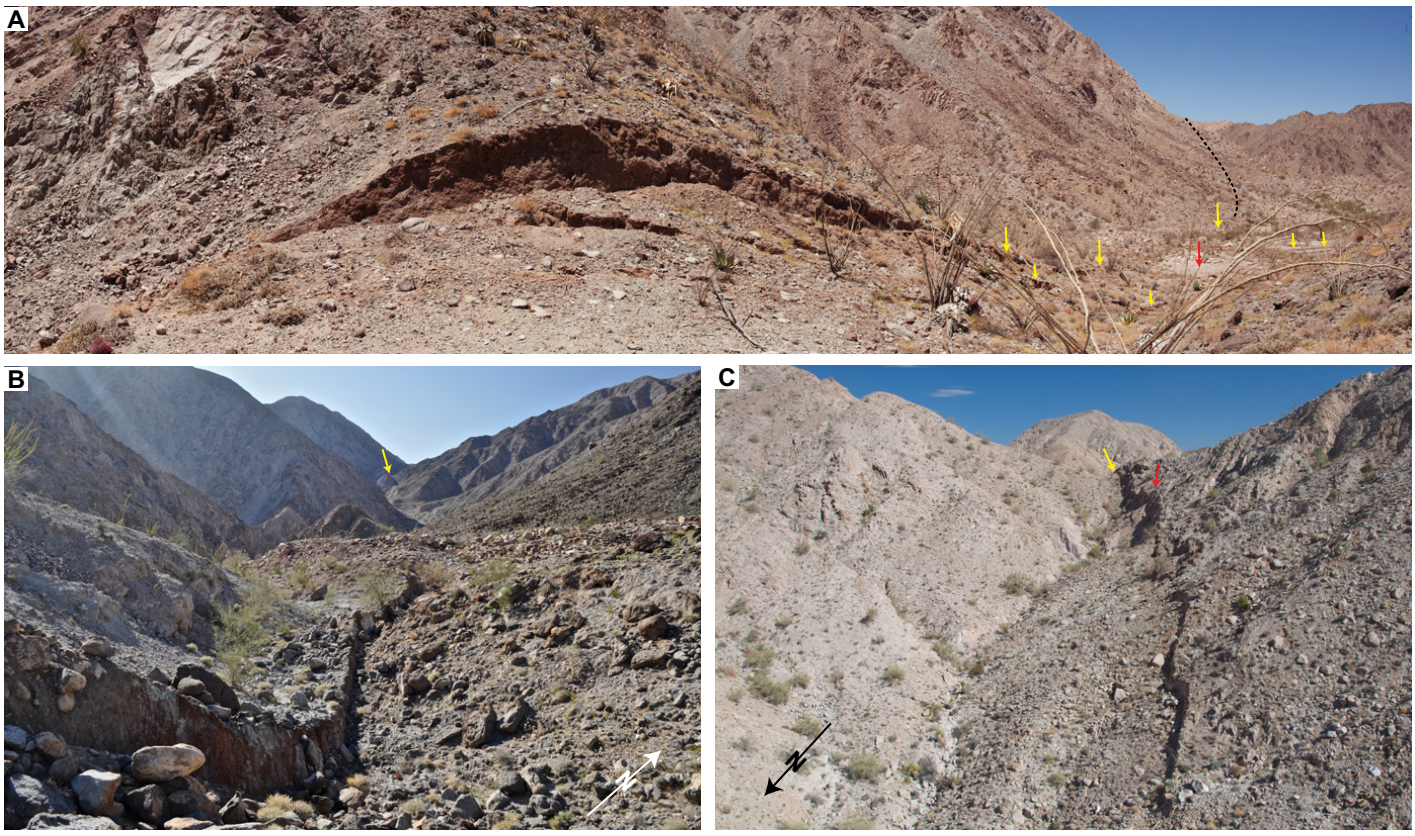

Figure 5. Field photos of Pescadores fault segment in the Sierra domain (photo locations plotted in Figure 3). (A) Rounded ridge in foreground is offset by ~235 cm of dextral and ~118 cm of northeast-side-down coseismic slip. Scarp height diminishes to left of ridge crest as this hillslope becomes subparallel to the southeast-plunging slip vector. Southwest-flowing drainages cross the Pescadores fault at high angles and previous surface ruptures have created short-lived dams that have captured ponded sediments (red arrow). Yellow arrows denote scarps in distance. Black dotted line is trace of the Pescadores fault. Photo azimuth is ~220°. (B) El Mayor–Cucapah (EMC) surface rupture on central portion of Pescadores fault segment. Scarp height is ~1 m in foreground. Rupture extends the length of the narrow fault valley that transects and blocks drainages. Profile of the Pescadores fault, which juxtaposes Mesozoic intrusive phases of different compositions, is visible in the distance (yellow arrow). Photo azimuth is ~315°. (C) EMC surface rupture along the northern Pescadores fault marked by yellow arrow (length of scarp in view is ~200 m). Recessed bedrock scarp formed in previous ruptures denoted by red arrow. Photos taken by John M. Fletcher. See Supplemental Files 1 and File 2 (see footnotes 1 and 2) for photo information in Google Earth KMZ format and table format, respectively.

monly located along distinct paleoscarps that define the limit of uplifted and abandoned alluvial fan surfaces (Fig. 6; Rymer et al., 2011). The kinematics of slip vary systematically with fault orientation, with northwest-striking faults dominated by right-lateral slip, northeast-striking faults dominated by left-lateral slip, and north-south faults largely accommodating vertical slip (Rymer et al., 2011). Offsets on individual surface ruptures in the Yuha Desert domain are small, varying from 2 to 8 cm, with a northward-decreasing gradient (Rymer et al., 2011); slip is thus two orders of magnitude less than is observed in the Sierra domain. In subsequent discussion herein we document the fact that most faults in the Yuha desert domain are located in the upper plate of a detachment fault that controls the northernmost segment of primary surface rupture in the Sierra domain, and likely forms the structural floor of this domain (Fig. 6).

Rymer et al. (2011) interpreted that surface rupture in the Yuha Desert domain is best described as triggered slip and distinct from primary slip observed farther south. In addition to dramatically lower magnitudes of slip, the domain is characterized by a much greater abundance of antithetic northeast-striking sinistral faults, and fracturing is distributed over a much wider region (Fig. 6). Nonetheless, the horsetail-style pattern of faulting is consistent with regional stress acting at the end of a major surface rupture with a significant component of right-lateral slip (e.g., Kim et al., 2004). Aftershocks of the EMC earthquake have a very high density in this region, and the largest aftershock (the M_w 5.8 June 15, 2010 earthquake) is located in the Yuha Desert domain, which is also consistent with the loading of faults at the ends of a major rupture.

The presence of paleoruptures with meter-scale offsets suggests that this domain has accommodated cross-faulting near the lateral limits of other major prehistoric ruptures (Fig. 6). Based on new mapping, it is now known that the 1892 rupture on the Laguna Salada fault also has a northern limit in this domain (Rockwell et al., 2010). Directly south of the Yuha Desert domain, in the northern part of the Sierra Cucapah, there are several major topographic and structural features that have the same northeast trend as many of the fault strands in the Yuha Desert domain. The most prominent of these is the Cerro Centinela, which is

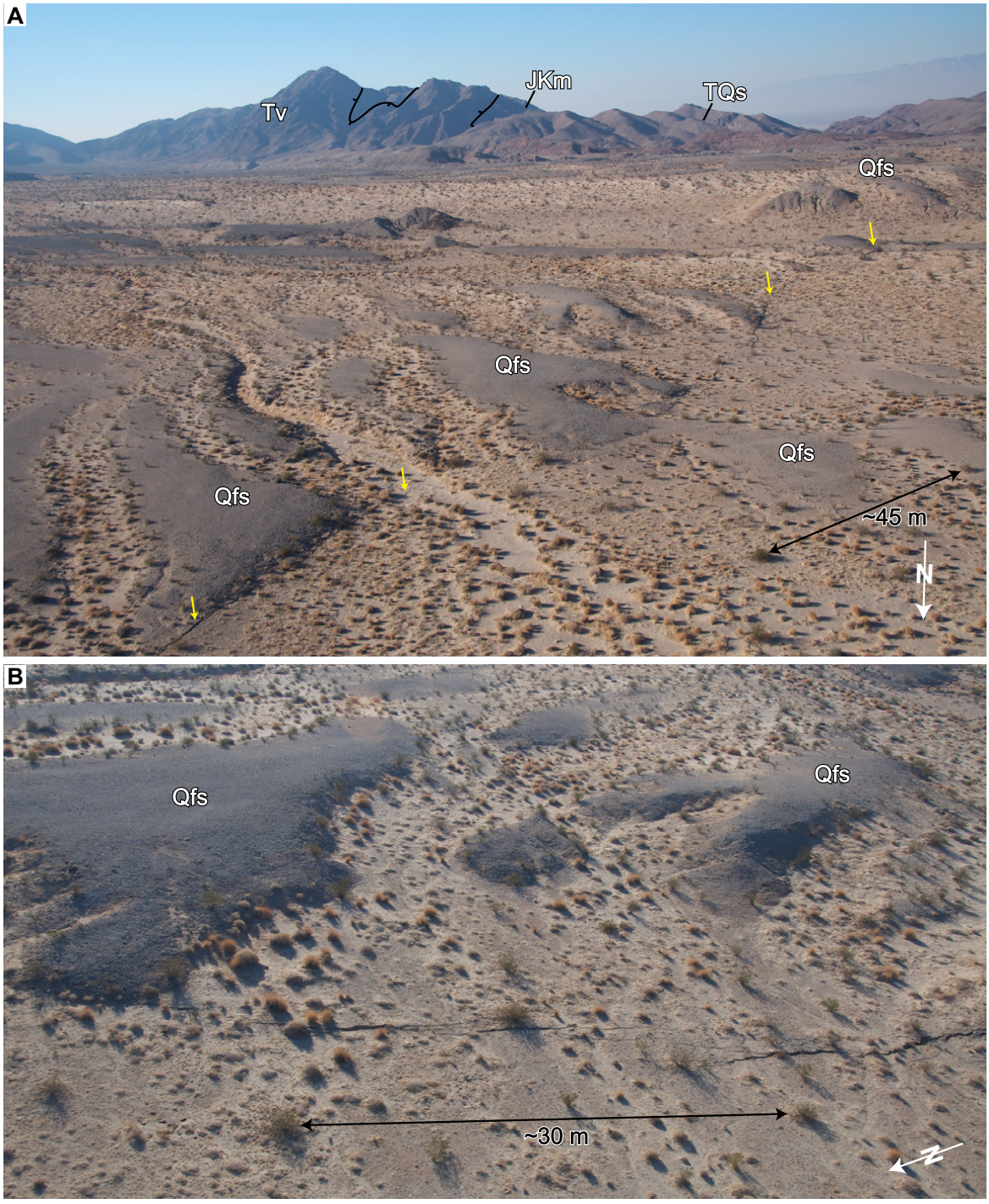

Figure 6. Oblique aerial photos of unnamed cross-fault in the Yuha Desert domain (photo locations plotted in Fig. 3; unit abbreviations as in Figure 7 legend). (A) Faults in the northernmost rupture domain cut a low-relief platform and uplift late Quaternary fan surfaces and basin fill (Qfs). Displacement associated with the rerupturing of paleoscarps (yellow arrows) in the Yuha Desert domain generally does not exceed 10 cm. Exposed in the distant high mountains is the Paso Superior detachment, which is the northernmost rupture controlling master fault in the Sierra domain. This fault separates Mesozoic gneissic rocks (JKm) from Neogene volcanic (Tv) and sedimentary rocks (TQs) in its hanging wall. The Paso Superior detachment projects into the subsurface toward the north and likely forms the structural floor of all faults in the Yuha Desert domain. Photo azimuth is ~165°. (B) El Mayor–Cucapah (EMC) rupture defined by fractures with right-stepping en echelon configuration formed along the base of a larger paleoscarp. Photo azimuth is ~125°. Photos taken by John M. Fletcher. See Supplemental Files 1 and 2 (see footnotes 1 and 2) for photo information in Google Earth KMZ format and Microsoft Excel table format, respectively.

a block of uplifted Mesozoic crystalline basement reaching more than 750 m in elevation with an elongated linear ridgeline oriented with an azimuth of ~020° (Fig. 3). Other fault-controlled northeast-trending ridgelines with lower relief are observed southeast of Cerro Centinela (Fig. 3). We interpret these features to collectively represent the limits of previous surface ruptures through the Sierra Cucapah. Thus the 2010 earthquake was anomalous in that it propagated farther to the north, beyond these more prominent northeast-striking faults.

2010 SURFACE RUPTURE IN THE SIERRA CUCAPAH

In the Sierra domain, EMC rupture activated slip on four different master faults that are separated by one branching intersection and two left-stepping accommodation zones (Fig. 7). From south to north, these are Laguna Salda fault, Pescadores fault, Puerta accommodation zone, Borrego fault, Paso Inferior accommodation zone, and Paso Superior fault (Fig. 7). In this section we summarize an extensive database of coseismic displacements as well as the orientation of master faults and scarps along the surface ruptures in the Sierra domain (Fig. 7). The master fault is the structure that has accommodated the finite geologic displacement, and its orientation in any given area is defined by the tectonic contact that juxtaposes distinct rock units from different fault blocks.

Master fault and scarp orientations were determined from outcrop measurements and three-point solutions of their traces on high-resolution airborne lidar-derived topography (Fig. 8). Three-point solutions were systematically collected along short, coplanar sections that transect topographic features such as channels and ridges. Individual scarps commonly occur in arrays of finite width that generally follow the master fault trace. However, the position of individual scarps varies along strike, and, in some cases, the entire coseismic scarp array is entirely located on one side of the master fault contact. Within any given array, individual scarps occur as distinct geometric and kinematic sets and thus some scarps were oriented oblique to both the scarp array and the master fault along which they propagated.

Rupture kinematics were characterized in the field by measuring the lateral and vertical components of offset markers across individual scarps (Fig. 9). The vertical component of slip was measured by projecting any displaced ground surface with a subhorizontal cutoff angle across the scarp (Figs. 10A–10C). Such markers were very common, which permitted us to make abundant reliable measurements of vertical offset. Offset markers that allowed a direct measurement of both the lateral and vertical components of slip included diverse geomorphic features such as bar and channel deposits, channel thalwegs, ridges, tread-riser intersections, shrub coppice dunes, as well as anthropogenic features that include tire tracks on a network of four-wheel drive roads, Highway 2, abandoned segments of Highway 2, boundaries of military rifle ranges marked by linear rows of painted boulders, animal tracks, and game trails (Figs. 9 and 10).

Total coseismic slip was determined by integrating individual measurements obtained in transects across the multiscarp rupture arrays. For each transect, total coseismic slip was calculated by a vector summation of the three components of slip (lateral, heave, and vertical) from each measurement (See Appendix 1 for more complete description of conventions and assumptions used in these calculations.) Transects were designed to be as comprehensive as possible, but in some locations not all components of slip could be measured due to the heterogeneous distribution of slip markers and/or incomplete exposure of the scarps. Therefore, some transects only integrate the vertical component and other transects only integrate the lateral components. Scarps with <5 cm of offset were not systematically measured by all geologists who contributed to the data slip database. Therefore, our measurements of total coseismic slip represent minimum estimates.

There are 335 measurements that represent our best estimates of the lateral and/or vertical components of total coseismic slip. In order to visualize along-strike variations in kinematics, integrated coseismic slip measurements were plotted as lines that scale in length with slip magnitude, as shown in Figure 11. Envelopes were superimposed on the measurements to visually smooth out high-frequency variations in slip and connect measurements that are most representative of the total slip magnitude.

All of the main data sets presented in this paper are included as supplemental material, and we have plotted each of them as separate layers of a KMZ file that can be viewed with Google Earth (see Supplemental File 1[1]). See Supplemental File 2[2] for geographic locations, view direction, and other information associated with all field photos used as figures in this paper. See Supplemental File 3[3] for a compilation of orientation data for scarp-forming faults and master faults. See Supplemental File 4[4] for field based measurements of coseismic slip across individual scarps as well as those integrated from transects across multiple scarps. See Supplemental File 5[5] for definitions of attribute field names used in tables and KMZ of the above mentioned supplemental material.

Laguna Salada Fault Segment

The Laguna Salada segment is the southernmost rupture segment of the Sierra domain and is closest to the epicenter (Fig. 11). The Laguna Salada rupture segment extends ~7 km from the edge of the Delta domain to the intersection with the Pescadores fault. At this branching fault intersection, most primary coseismic slip becomes partitioned onto the Pescadores fault and other faults of the east-dipping imbricate array (Fig. 11). However, minor rupture, not exceeding 30 cm, continues to the northern limit of the EMC rupture on the west-dipping Laguna Salada fault, and thus most of the length of the 1892 rupture (M_w 7.2) was reactivated in 2010 (Figs. 7 and 12).

Based on the location of the epicenter, the rupture is likely to have propagated to the northwest through the fault array in the Sierra Cucapah. However, slip on the southeasternmost Laguna Salada fault is divided into two splays that merge toward the northwest (Fig. 11). This merging of rupture in the direction of propagation may be due to the focusing of seismogenic slip from the more broadly distributed shearing in the Delta domain. The dip of the Laguna Salada fault is steep to subvertical along most of its length, and dip direction changes along strike (Mueller and Rockwell, 1991). The strike of the

[1]Supplemental File 1. Google Earth KMZ file containing the main datasets and geolocated photographs. The .kmz file can be viewed in Google Earth. If you are viewing the PDF of this paper or reading it offline, please visit http://dx.doi.org/10.1130/GES00933.S1 or the full text article on www.gsapubs.org to view Supplemental File 1.

[2]Supplemental File 2. Photo information in Microsoft Excel table format. If you are viewing the PDF of this paper or reading it offline, please visit http://dx.doi.org/10.1130/GES00933.S2 or the full text article on www.gsapubs.org to view Supplemental File 2.

[3]Supplemental File 3. Orientation of scarp-forming faults and master faults in Microsoft Excel table format. If you are viewing the PDF of this paper or reading it offline, please visit http://dx.doi.org/10.1130/GES00933.S3 or the full text article on www.gsapubs.org to view Supplemental File 3.

[4]Supplemental File 4. Field measurements of coseismic displacements across fault scarps in Microsoft Excel table format. If you are viewing the PDF of this paper or reading it offline, please visit http://dx.doi.org/10.1130/GES00933.S4 or the full text article on www.gsapubs.org to view Supplemental File 4.

[5]Supplemental File 5. Table defining attribute field names used in tables and KMZ of supplemental material. If you are viewing the PDF of this paper or reading it offline, please visit http://dx.doi.org/10.1130/GES00933.S5 or the full text article on www.gsapubs.org to view Supplemental File 5.

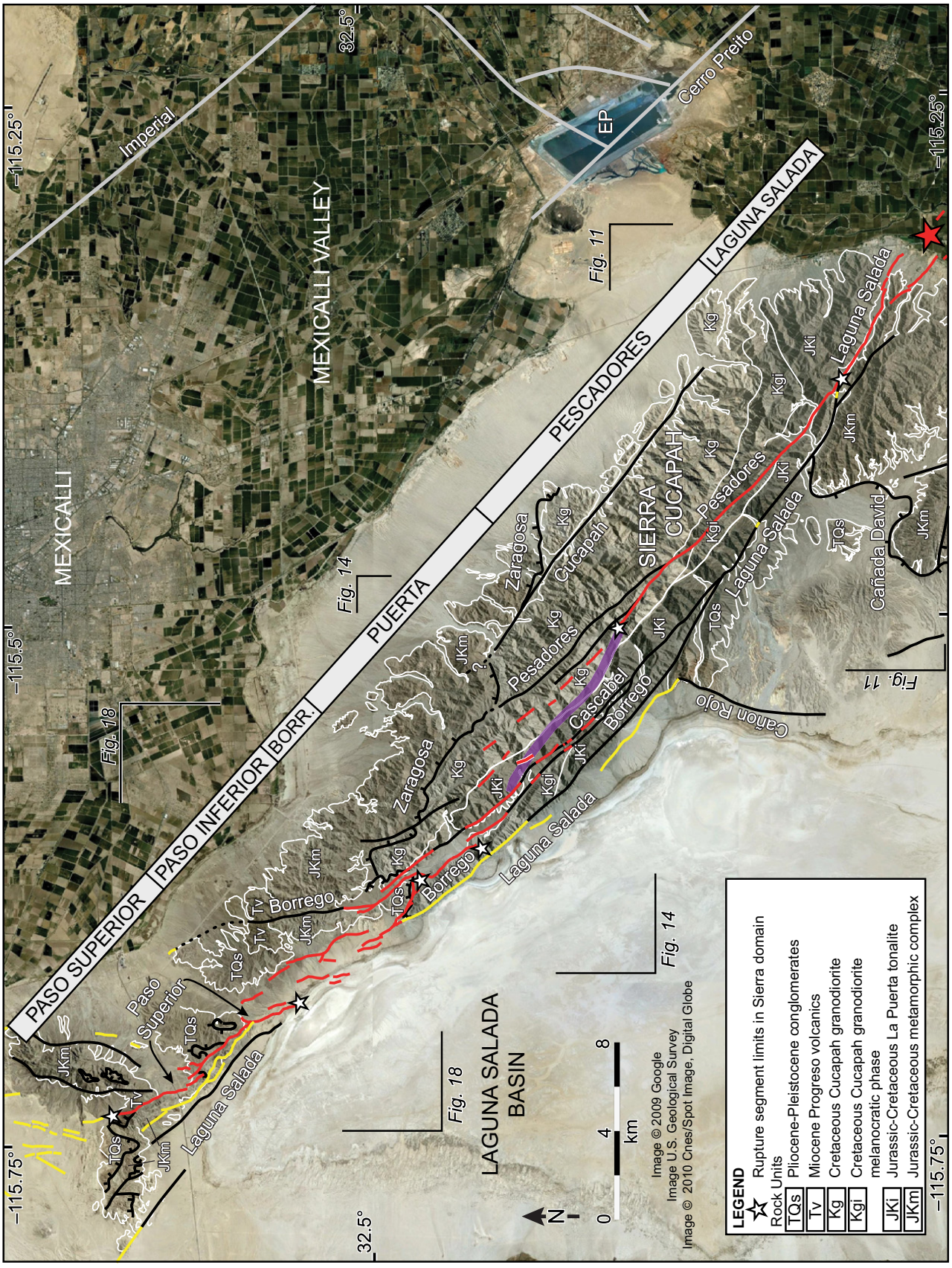

Figure 7. Geologic map of the Sierra Cucapah showing (1) schematic major (red) and minor (yellow) rupture traces, (2) faults (in black), and (3) lithologic contacts in white. Purple line delineates a gradient in surface displacement detected by COSI-Corr (co-registration of optically sensed images and correlation) pixel tracking (see text section on Puerta accommodation zone for more details). White stars define exact locations of main rupture segment boundaries labeled along the northeast margin of the Sierra Cucapah. EP—evaporation pond of the Cerro Prieto geothermal field.

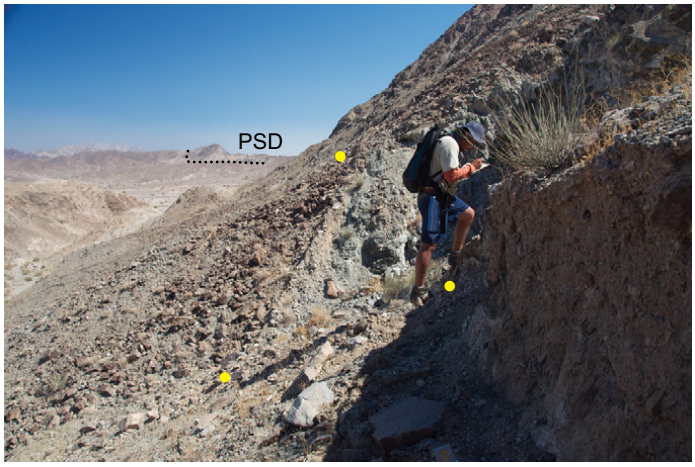

Figure 8. The strike and dip of faults and scarp dips were systematically determined along the length of the rupture in the Sierra domain using both outcrop measurements and lidar (light detection and ranging) based three-point solutions in places where the planar surfaces transected topographic features such as channels and ridges (yellow dots in photo). The scarp in this photo dips ~56° along a ramp section of the Paso Superior detachment (PSD). Photo taken by John M. Fletcher. See Supplemental Files 1 and 2 (see footnotes 1 and 2) for photo information in Google Earth KMZ format and Microsoft Excel table format, respectively.

Laguna Salada fault within this rupture segment ranges from 285° to 310°, and thus this rupture segment has the most westerly striking faults in the entire rupture array.

Total slip reaches a maximum of 331 cm and is dominated by right-lateral displacement (Fig. 11). Some sections of the Laguna Salada fault have no measurable vertical offset. Where vertical offset is observed, it is generally <30 cm and changes polarity from northeast side down to southwest side down along strike. The most common offset features observed in this segment were recent bar and channel deposits located along the active drainage (Fig. 10D). Displacement estimates were difficult to determine in places where the fault array was subparallel to bar and channel morphology.

Pescadores Fault Segment

The Pescadores segment extends ~15 km along strike and is the longest segment where rupture is controlled by and confined to a single master fault (Fig. 11). The trace of the Pescadores fault follows closely along the western flank of the topographic axis of the Sierra Cucapah, reaching the highest elevations and the most remote locations along the entire surface rupture. The Pescadores fault strikes 300° to 320°. In contrast to the Laguna Salada fault, the Pescadores fault shows no changes in polarity of dip and dips steeply to the northeast along its entire length (Figs. 5 and 11).

Although the strike of the Pescadores fault is very similar to that of the Laguna Salada fault, the kinematics of rupture undergoes a marked change at the intersection of the two faults and vertical slip increases and is systematically northeast-side down along the entire length of this segment (Fig. 11). Locally, there are southwest-down scarps, but these were always antithetic and minor in magnitude compared to the northeast-down slip. It is interesting that this sense of vertical slip is inverse to the modern topography and lowers the very highest part of the Sierra Cucapah along the entire length of the

Figure 9. Field photo showing kinematics of the El Mayor–Cucapah rupture: offset riser-tread intersections and channel thalweg provide excellent piercing points to measure coseismic displacement (channel thalweg displaced ~320 cm dextral and ~100 cm vertical; yellow markers displaced ~270 cm dextral and ~130 cm vertical; red markers displaced ~170 cm dextral and ~50 cm vertical). Slip vector is slightly steeper than hillslope with red markers at the top. Photo azimuth is ~220°. Photo taken by John M. Fletcher. See Supplemental Files 1 and File 2 (see footnotes 1 and 2) for photo information in Google Earth KMZ format and table format, respectively.

segment (Fig. 11). The Pescadores scarp array locally dams nearly every southwest-flowing drainage that crosses it, and shutter ridges formed by multiple events with displacements similar to the M 7.2 EMC earthquake are common (Fig. 5). In the Pescadores segment, right-lateral slip is 2–4 times greater than vertical displacements and net slip reaches 381 cm. Much of the Pescadores surface rupture is located along very steep slopes composed of coarse boulder deposits and colluvium (Fig. 5). Coseismic slope failure erased evidence for large sections of the scarp array and made finding offset markers difficult. Nonetheless, offset features such as channels, ridges, and alluvial deposits were common near large drainages, which is where most of the field measurements of slip are concentrated (Figs. 10G and 11). The Pescadores rupture segment is kinematically one of the most homogeneous of the scarp array.

Pescadores Fumarole

One of the most surprising rupture-related phenomena found along this segment is an active fumarole that appeared in a wide alluviated valley near the southern end of the Pescadores fault (Figs. 11 and 13). The Pescadores fumarole constantly emits a prominent vapor cloud that can be seen from distances of several kilometers, and the vapor cloud occasionally rises above nearby peaks before evaporating into the dry desert air. In addition to vapor, the fumarole also extrudes a dusting of altered rock particles that blanket the ground around the vent (Fig. 13). The most active vent measures 1.5 m in diameter and steam was also emitted from fractures and through coarse clastic deposits within 5 m of the main vent. Penetrative ground cracking was observed around the vent, which is located within 10 m of the coseismic rupture (Fig. 13). The fumerole is located along a subtle right-stepping deflection of the rupture trace, and thus its location may be controlled by a releasing bend in the Pescadores fault. The fumarole site is ~16 km from the Cerro Prieto geothermal field, and magnetotelluric profiles demonstrate the existence of shallow geothermal anomalies that approach the southeast margin of the Sierra Cucapah (Fig. 11; Cortes-Arroyo, 2011). Dilatation of rock volume associated with the rupture activity (e.g., Morton et al., 2012) as well as the subtle releasing bend geometry of the Pescadores fault likely provided conduits and mobilized fluids to produce the observed fumerole.

The Pescadores fumarole does not appear in long-distance photographs and was not otherwise observed in helicopter surveys performed in the days immediately following the EMC earthquake. Therefore hydrothermal activity at the site might not have initiated for days or weeks after the rupture. However, by 27 April 2010 the fumarole was vigorously active when field geologists (this study) first visited this section of the Pescadores fault. Colleagues at the Comisión Federal de Electricidad associated with the Cerro Prieto geothermal field were informed of the fumarole within months of its discovery and consider it to be a new geothermal field in Baja California (Alvarez-Rosales et al., 2012). Barnard (1968), who was the first to map and name most of the faults in the Sierra Cucapah, reported that the ground was hot to touch in some of the fault-controlled valleys in the southernmost part of the range. However, to our knowledge, historical activity of the fumarole has not been previously documented. Nonetheless, hydrothermally altered rock particles similar to those seen on the surface are found entrained in late Quaternary alluvial deposits around the fumarole, suggesting that it is a relatively long lived hydrothermal perturbation with previous periods of activity possibly related to other ruptures on the Pescadores fault.

Puerta Accommodation Zone

The Puerta accommodation zone exhibits complex faulting where surface rupture is transferred in a left-stepping manner from the Pescadores fault to the Borrego fault (Fig. 14). These two master faults are only separated by an across-strike distance of 2–3 km, but the distance along strike separating points where slip is entirely consolidated on a single master fault is ~10 km. Near the northern end of the Pescadores segment, the Pescadores fault bifurcates and rupture follows the structurally lowest strand for ~3.5 km before abruptly terminating in a region slightly removed from the master fault trace (Fig. 11). Surface rupture with minor net coseismic slip appears on the Borrego fault within a distance of ~3 km from the termination of Pescadores fault segment. However, slip on the Borrego fault within the northern half of the accommodation zone is discontinuous and kinematically dominated by dip slip, which reflects the partitioning of slip onto other structurally higher faults. Both the Borrego and Pescadores faults dip to the east and form the structural roof and floor of the accommodation zone. However, because the Borrego fault generally dips at a shallower angle than the Pescadores fault, they should intersect at depths of 10–12 km. Therefore, the two master faults are not spatially isolated, but rather they are likely hard linked at depth.

The Cascabel fault is the only other previously mapped structure to accommodate surface rupture besides the Borrego fault and Pescadores fault. The Cascabel fault is an antithetic fault in the east-directed system and bounds the northeast margin of a narrow rift basin in the hanging wall of the Borrego fault. Throughout the southern half of the narrow rift basin, the sequence of Pleistocene gravels and Palm Spring formation together with the graben-bounding faults

Figure 10 (*on following page*). Field photos showing some of the planar and linear markers used to measure offset across scarps of the El Mayor–Cucapah (EMC) rupture. (A) Vertical offset of ~70 cm measured by projecting sloping ground surface across scarp formed on Pescadores fault. (B) An offset alluvial fan surface along the Borrego fault, which has vertical offset of ~275 cm formed entirely in the EMC earthquake. (C) Offset tire tracks (excellent piercing points) showing ~33 cm vertical and ~24 cm of sinistral displacement on one of the strands of a north-northeast–striking scarp array in the Paso Inferior accommodation zone. (D) The edge of a boulder deposit formed along the margin of a modern channel (marked by red dashed lines) is offset ~330 cm in a dextral sense along the Laguna Salada fault. No vertical offset observed at this site. (E) Row of white painted boulders used to mark the sides of a military rifle range is offset dextrally along the Paso Superior detachment (~134 cm dextral and ~50 cm east-down vertical offset measured here). (F) Coseismic slip distributed across multiple strands displace painted markers of Highway 2 along the Paso Superior detachment (~120 cm dextral and ~52 cm east-down vertical offset measured here). (G) Small ridgeline records ~340 cm dextral and ~65 cm vertical offset along the Pescadores fault. Shallowly plunging striae developed in clay gouge of bedrock scarp follow the displacement vector of the EMC rupture. Curving striae on lower portion of the scarp face may have formed adjacent to clasts that were not firmly attached to the opposing block. (H) Ridgeline along the Paso Superior detachment is offset with ~230 cm dextral and ~50 cm vertical slip. Shallowly plunging striae in gouge of bedrock outcrop define the coseismic slip direction. (I) Offset lizard tracks indicate ~3 cm of dextral and ~33 cm of vertical slip. A, B, D, G, and H taken by John M. Fletcher; C, E, and I taken by Orlando J. Teran; F taken by Ronald M. Spelz. See Supplemental Files 1 and 2 (see footnotes 1 and 2) for photo information in Google Earth KMZ format and Microsoft Excel table format, respectively.

Figure 10.

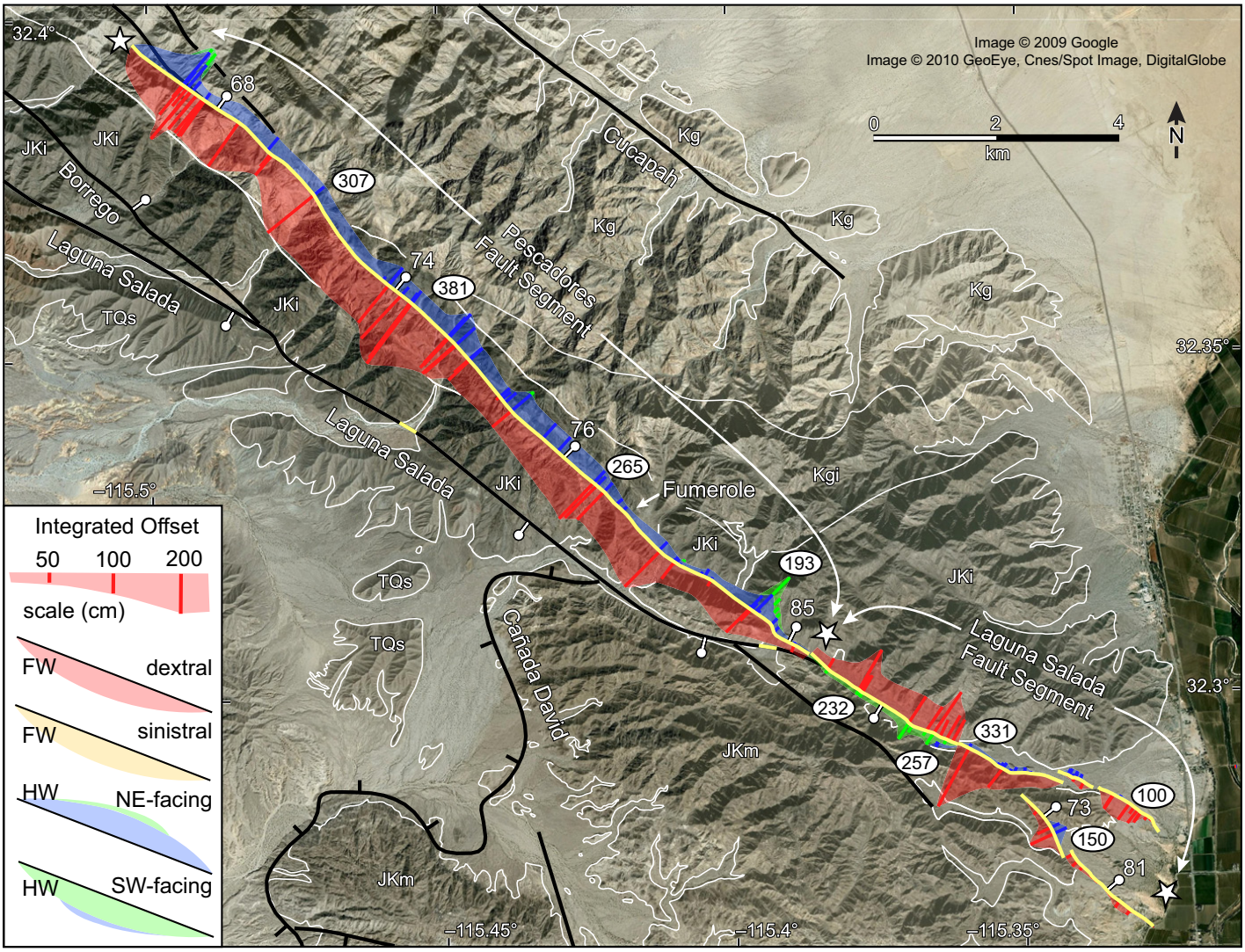

Figure 11. Geologic map of the southern Sierra Cucapah showing schematic rupture traces (yellow lines) and distribution and magnitude of displacement measurements. White ellipses contain integrated total slip estimates (in centimeters) for groups of field measurements made in transects. Slip components are plotted as line symbols scaled to slip magnitude. Lateral and vertical components of slip are plotted in the footwall (FW) and hanging wall (HW), respectively. Shaded envelopes show along-strike variations in slip magnitude and extrapolate across the high and intermediate peaks in field slip data. White stars mark the limits of the Laguna Salada and Pescadores fault segments. Southernmost rupture segment is controlled by the Laguna Salada fault. Unit abbreviations as in Figure 7 legend.

have been tilted 20°–30° to the west such that this portion of the west-directed Cascabel fault has been rotated through vertical and now dips steeply to the east (Fig. 15A). Throughout the accommodation zone, the Cascabel fault records as much as 163 cm of oblique dextral and east-side-down slip. This sense of vertical slip reverses the west-down finite displacement of the fault, and thus is an excellent example of how faults change in kinematics as they rotate to new orientations during progressive shearing. Another example of mechanical interactions between the Casacabel and Borrego faults is the kinematic partitioning of coseismic slip. Although both accommodate east-down normal slip, the Borrego surface rupture in this accommodation zone has no lateral offset (Fig. 15B). Instead the lateral component of coseismic slip is partitioned onto other structurally higher fault strands like the Cascabel that that dip more steeply and sole into the Borrego fault.

Much of the evidence for the kinematics and distribution of surface rupture was erased by coseismic slope failure in a manner similar to that observed along the Pescadores fault. Coseismic mass wasting eroded many sections of the surface rupture and its deposits buried others (Fig. 16). The complex distribution of surface rupture among numerous discrete faults along with the lack of preservation has made it nearly impossible to characterize surface rupture in the accommodation zone by field observations alone. Instead, the distribution of surface rupture in the accommodation zone was largely documented by satellite image differencing (S. Wei et al., 2011). Many of the surface ruptures through the accommodation zone occur on faults that either do not juxtapose different rock units or do not significantly offset lithologic contacts.

A prominent gradient in surface displacement, as detected with COSI-Corr (co-registration of optically sensed images and correlation)

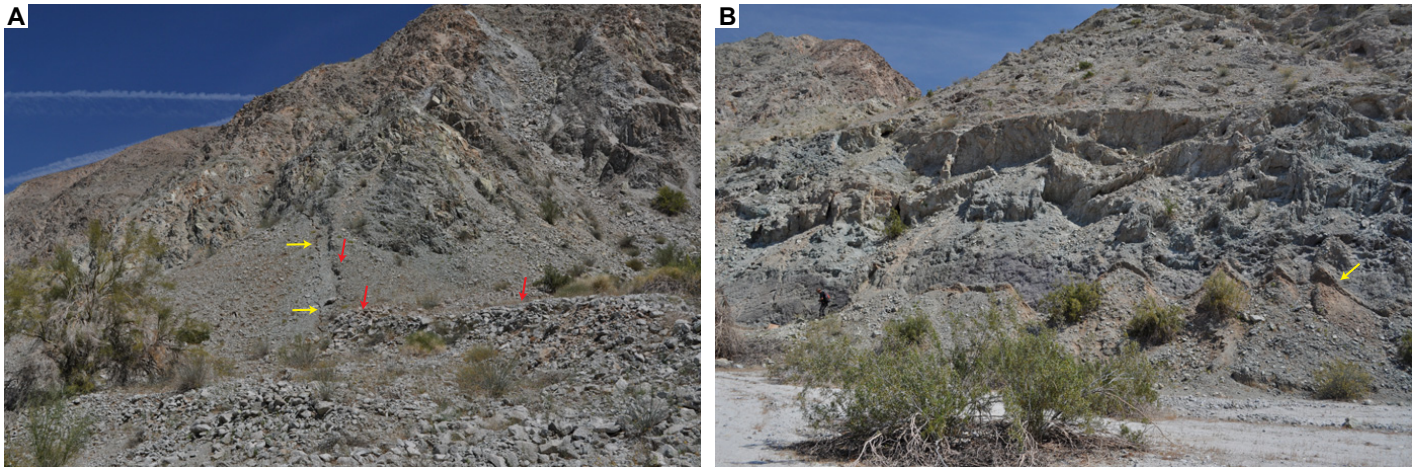

Figure 12. Photos showing El Mayor–Cucapah (EMC) surface rupture along the basin-bounding segment of the northern Laguna Salada fault. As much as 30 cm of west-down normal slip with no lateral component was accommodated by EMC rupture that closely followed base of larger scarps formed in 1892 (Mueller and Rockwell, 1991). (A) Red arrows point to the top of the 1892 scarp, which cuts alluvial fan and hill slope deposits and accommodated as much as ~350 cm of oblique dextral normal displacement. Yellow arrow marks fractures (~10 cm of vertical displacement) formed in the EMC rupture. Photo azimuth is ~005°. (B) EMC rupture follows base and incrementally uplifts bedrock scarp that formed in 1892. Small ridge crests show ~30 cm of vertical displacement, but no systematic sense of lateral offset across EMC rupture. Photo azimuth is ~040°. Photos taken by John M. Fletcher. See Supplemental Files 1 and File 2 (see footnotes 1 and 2) for photo information in Google Earth KMZ format and table format, respectively.

Figure 13. Field photo of fumarole observed along the Pescadores fault segment (location of fumarole shown in Fig. 11). Main vent has a diameter of ~3 m and is surrounded by dusting of pale pink extruded solid particles. Main vent is located within 20 meters of the trace of the El Mayor–Cucapah coseismic rupture (yellow arrows). A side vent located on the modern ground surface (vertical red arrow) became inactive prior to this photo being taken (13 August 2010). Horizontal red arrow indicates ash-like particles entrained in older alluvium indicating previous late Quaternary hydrothermal activity at this site, perhaps associated with the penultimate rupture. Photo azimuth is ~270°. Photo taken by John M. Fletcher. See Supplemental Files 1 and File 2 (see footnotes 1 and 2) for photo information in Google Earth KMZ format and table format, respectively.

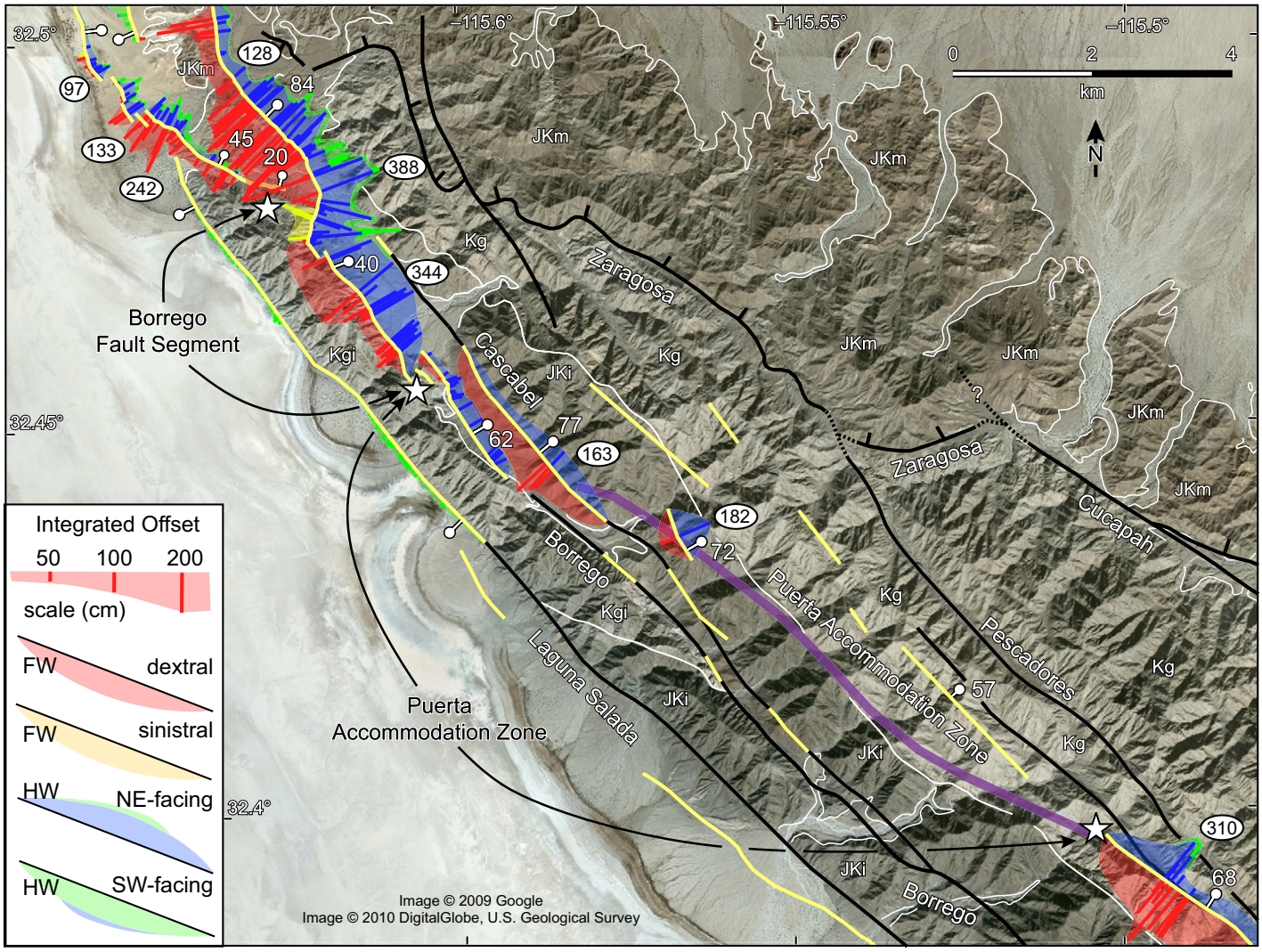

Figure 14. Geologic map of the central Sierra Cucapah showing schematic rupture traces (yellow lines) and distribution and magnitude of coseismic displacements measured in the field. White ellipses contain integrated total slip estimates (in centimeters) for groups of field measurements made in transects. Slip components are plotted as line symbols scaled to slip magnitude. Lateral and vertical components of slip are plotted in the footwall (FW) and hanging wall (HW), respectively. Shaded envelopes show along-strike variations in slip magnitude and extrapolate across the high and intermediate peaks in field slip data. Purple line delineates a gradient in surface displacement detected by COSI-Corr (co-registration of optically sensed images and correlation) pixel tracking (see text for details). White stars demarcate limits of the Puerta accommodation zone and Borrego fault segment. Unit abbreviations as in Figure 7 legend.

processing of pre-event and post-event SPOT satellite images, extends across nearly the entire length of the Puerta accommodation zone (S. Wei et al., 2011). In other parts of the Sierra domain, such gradients typically correspond to ruptured master faults. Given the poor preservation of scarps in this segment, it is certainly possible that the gradient corresponds to a continuous coseismic rupture that extends ~9 km. However, the gradient passes across, but does not appreciably displace a prominent intrusive contact marking the outer margin of the Cucapah granodiorite. Therefore, if this is a continuous fault, it likely has low finite offset (< 1 km).

Borrego Fault Segment

The 2010 rupture on the Borrego fault extends >10 km, but because it is flanked by accommodation zones where slip is partitioned among multiple master faults, we define the Borrego segment to only include the central portion where slip is localized on a single master fault (Fig. 14). Despite being the shortest master fault segment, extending only ~3 km along strike, the Borrego fault rupture has the most diverse range of geometry and kinematics. The strike of the Borrego fault varies from 320° to 015°, and its curvilinear trace likely reflects the linking of misaligned fault segments (e.g., Ferrill et al., 1999) and the development of megamullion corrugations (undulations of the fault surface) such as those that are commonly found on basin-bounding normal faults with large displacements (>5 km; e.g., Axen, 2007).

In this rupture segment, the Borrego fault zone is generally more than 50 m wide and dips moderately (as low as 40°; Figs. 14 and 17A). Due to the broad width and moderate inclination of the master fault, damaged and altered fault zone rocks are commonly observed along the entire mountain flank of the uplifted footwall

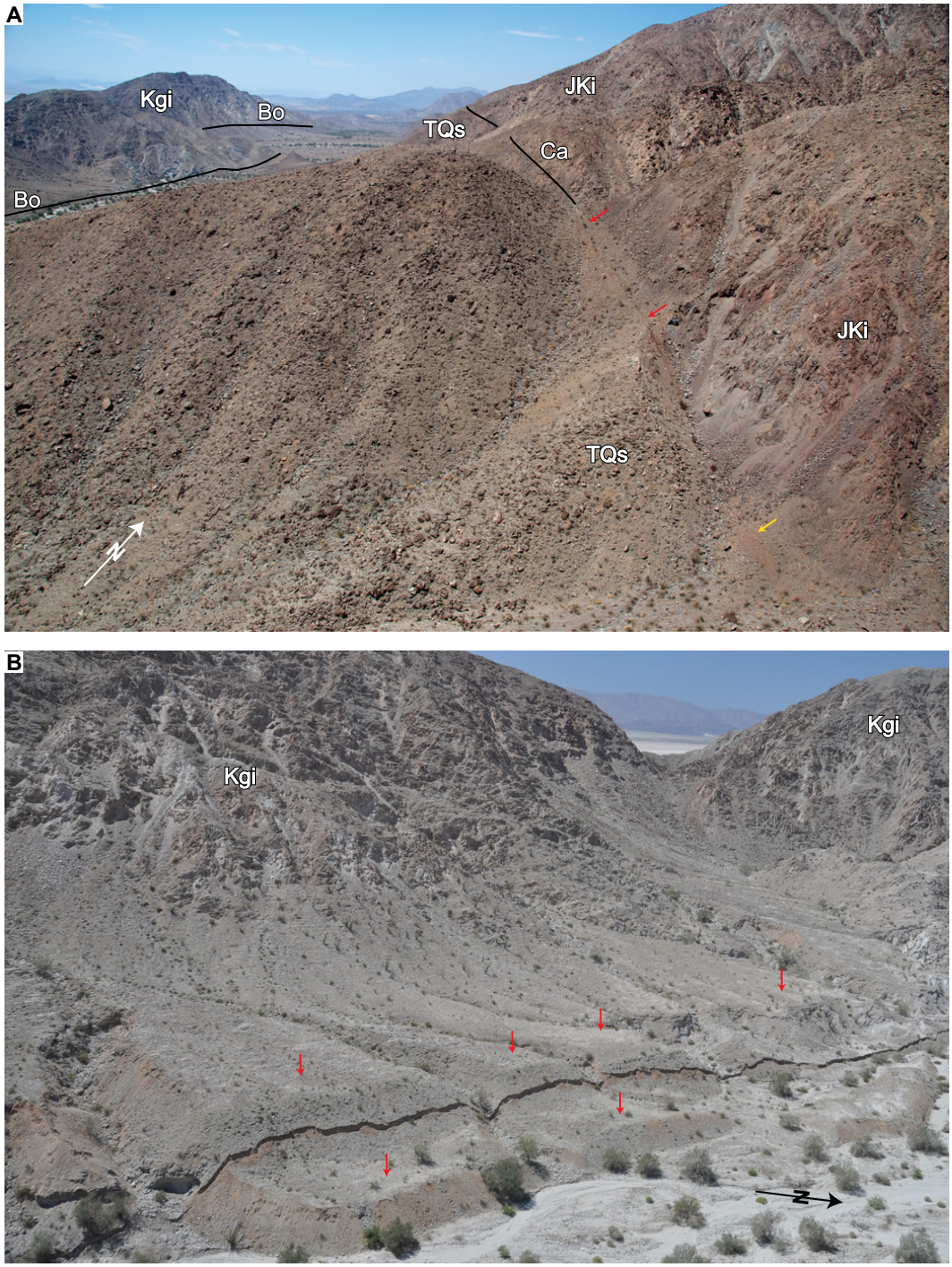

Figure 15. Field photos of kinematic partitioning of surface rupture between the Borrego (Bo) and Cascabel (Ca) faults in the northern Puerta accommodation zone. (A) The Borrego and Cascabel faults control a narrow rift basin and juxtapose Mesozoic crystalline basement (JKi) with Pliocene–Pleistocene conglomeratic basin fill (TQs). In this photo, both faults dip east, but the dip direction of the Cascabel fault has been inverted by progressive westward tilting in the hanging wall of the Borrego fault (see text). Coseismic displacements measured at locations marked by red arrows have ~180 and ~135 cm of dextral shear and ~90 cm of east-down normal shear. The east-down sense of coseismic dip slip is opposite to the finite, geologic, west-down slip of the Cascabel fault. Photo azimuth is ~315°. Black lines mark master fault traces. (B) El Mayor–Cucapah surface rupture pierces the center of paleooscarp on the Borrego fault and accommodates pure normal-sense dip slip. The strike-slip component of coseismic slip is accommodated by other faults like the Cascabel fault in this portion of the Puerta accommodation zone. The late Quaternary fan surface (marked by red arrows) has been displaced ~10 m by the last three surface ruptures on this fault segment (Hernandez et al., 2013). Photo azimuth is ~265°. Photos taken by John M. Fletcher. See Supplemental Files 1 and 2 (see footnotes 1 and 2) for photo information in Google Earth KMZ format and Microsoft Excel table format, respectively.

block. Therefore, the Borrego fault segment can be classified as a mountain-flank fault, which distinguishes it from a mountain-front fault (e.g., Cichanski, 2000). Because the scarps from the EMC earthquake are distributed throughout the width of the fault zone and also dip at moderate angles, they form a distinctive pattern of surface rupture that we designate as a mountain-flank scarp array (Fig. 17).

The topography along the Borrego fault segment is not as extreme as observed in the Pescadores segment and Puerta accommodation zone and, in general, scarp traces are very well preserved. Nonetheless, alluvial fan surfaces are moderately inclined and the deposits are very coarse grained, and lateral displacements were best defined by offset modern channels. The coseismic kinematics of the Borrego rupture segment are dominated by oblique dextral northeast-down normal slip, which reaches 344 cm in magnitude (Fig. 14). Near the northern limit of

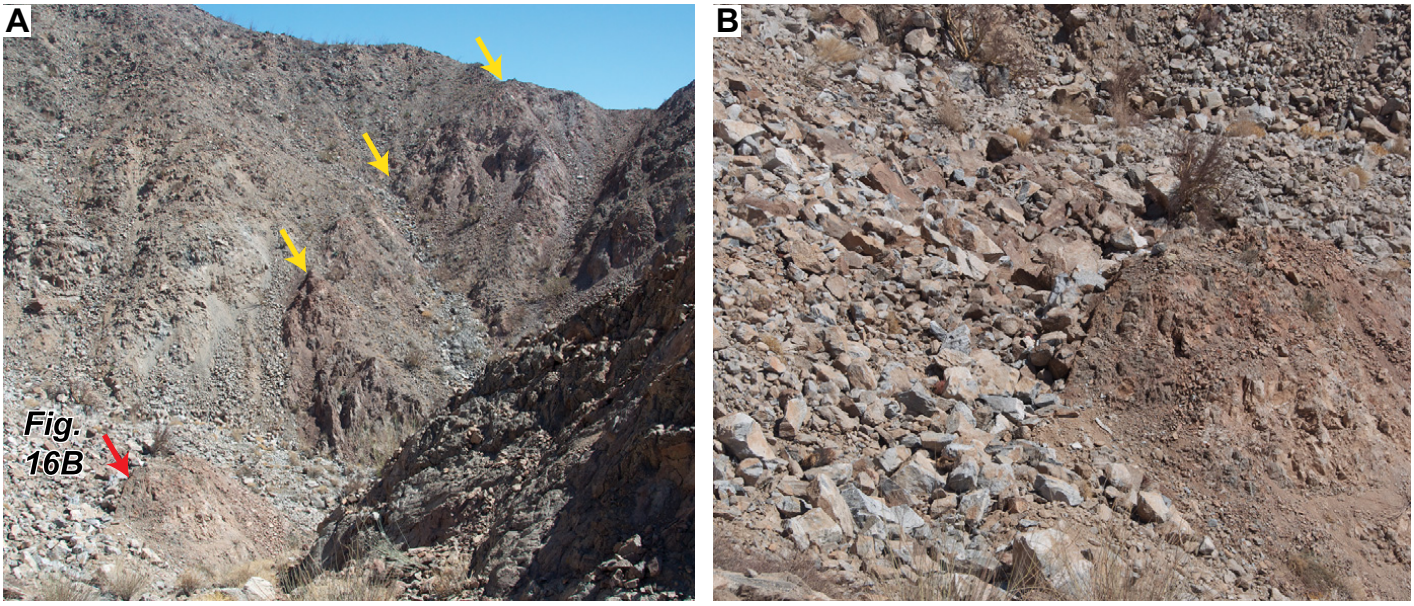

Figure 16. Field photos of unnamed fault in the Puerta accommodation zone. (A) Trace of the surface rupture (yellow arrows) is discontinuous because many parts were destroyed by coseismic landslides that occurred on the steep mountain slopes. Photo azimuth is ~135°. (B) Angular boulder clasts of coseismic landslide deposits partially bury scarp (height is ~125 cm) in the base of the canyon. Photos taken by John M. Fletcher. See Supplemental Files 1 and File 2 (see footnotes 1 and 2) for photo information in Google Earth KMZ format and table format, respectively.

the rupture segment, an abrupt change in strike to the northeast coincides with a reversal in the sense of relative lateral offset to sinistral and an abrupt increase in the magnitude of antithetic southwest down vertical offset (Fig. 14).

Paso Inferior Accommodation Zone

The Paso Inferior accommodation zone is located along the margin of the Laguna Salada lake bed; it extends ~6 km along strike and has a width of ~2 km (Fig. 18). In contrast to the Puerta accommodation zone, the complexities of faulting and the nature of slip transfer between discrete faults are well preserved and well exposed. The accommodation zone has very low relief and even the uplifted blocks of many fault strands are buried beneath modern alluvium, which suggests that this segment of the surface rupture is dominated by subsidence. The southern limit of the Paso Inferior accommodation zone is located at the intersection of a low-angle detachment fault with the central portion of the Borrego fault, which is where coseismic rupture bifurcates (Fig. 19). One splay follows the curvilinear trace of the detachment in a more western direction (Figs. 18 and 19). The detachment dips 20°–45° to the northeast and forms the westernmost strand and structural floor of the Paso Inferior accommodation zone (Figs. 18 and 19A). The other splay follows the northward continuation of the Borrego fault, which forms the structural roof of the Paso Inferior accommodation zone (Fig. 18). The northern limit of the Paso Inferior accommodation zone is located where coseismic rupture reconsolidates on a fault that we have named the Paso Superior detachment (Fig. 18).

The geometry of the Borrego fault changes markedly at its intersection with the southern detachment fault, and to the north it becomes much steeper (70°–84°; Fig. 18). The change in geometry coincides with a change in rupture array architecture, and the wide mountain flank scarp array observed to the south (Fig. 17) collapses to a much narrower array with a well-defined principal scarp (Fig. 20A). However, a significant component of antithetic southwest-down vertical slip is also observed immediately adjacent to the northern Borrego fault (Fig. 18), and more antithetic slip is spatially partitioned onto the Cascabel fault a few hundred meters to the east.

The kinematic and geometric diversity of faulting in the Paso Inferior accommodation zone surpasses that observed in any other segment of the surface rupture. Here, three main fault strands accommodate the transfer of slip from the Borrego fault to the Paso Superior detachment. The main fault strands show a range in strike of 300°–020° and dips that range from 20° to 84° (Fig. 18). Despite the partitioning of slip, the magnitude of coseismic slip actually increases to 388 cm on the northern Borrego fault (Fig. 18), and is the maximum observed on a single master fault. However, within ~2 km of this maximum slip section, rupture on the Borrego fault dies out altogether and becomes transferred to structurally lower faults located to the west (Fig. 18). The detachment fault in the southernmost Paso Inferior accommodation zone is the structurally lowest fault strand and shows both right-lateral strike slip and predominantly east-side-down vertical slip (Fig. 18). A significant number of scarps with southwest-down antithetic slip were also observed in this array. Net coseismic slip on the detachment is very low (<10 cm) near the intersection, but increases to a maximum of 242 cm (Fig. 18). From this maximum slip location toward the north, coseismic slip progressively diminishes as it becomes transferred to a prominent west-side-down antithetic fault that forms a small graben in the region where they overlap (Figs. 18 and 20B). The trace of the west-dipping fault is located along the edge of uplifted hills of gravelly basin fill, and it also controls the western limit of a narrow horst block of Mesozoic crystalline rocks in the footwall of the Borrego fault (Figs. 18 and 20B). Surface rupture on this fault persists for more than 4 km, which is nearly the entire length of the accommodation zone, before it dies out and is transferred to a much shorter, west-side-down fault at the northern limit of the accommodation zone (Fig. 18). Both of these west-dipping faults are almost completely

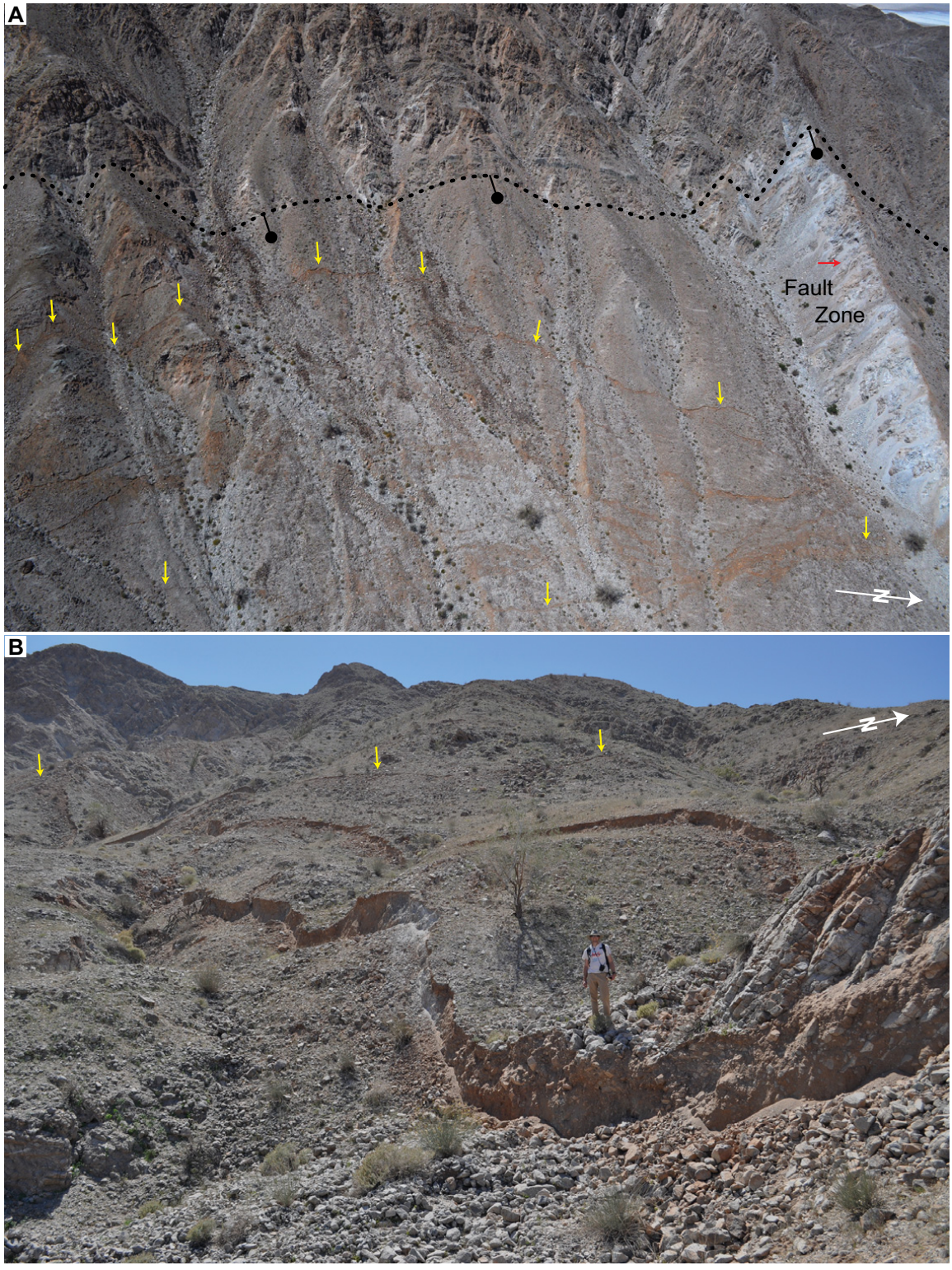

Figure 17. Field photos of the Borrego fault segment in the Sierra Domain. (A) Mountain flank scarp array on the Borrego fault. Fault zone (labeled in photo) is ~50 m thick, composed of breccia, gouge and cataclasite and is inclined at angles (~45°; ball and bar symbols show dip direction) that are only slightly greater the mountain flank hillslope (red arrow). The array of scarps (yellow arrows) climbs the mountain flank and reaches the base of the fault zone (black dotted line). Photo azimuth is ~250°. (B) Scarps expose weathered colluvium and basement-derived cataclastic rocks in uplifted free faces. Geologist is ~190 cm tall. The highest scarps (yellow arrows) coincide with the base of the cataclastic shear zone. Photos taken by John M. Fletcher. See Supplemental Files 1 and File 2 (see footnotes 1 and 2) for photo information in Google Earth KMZ format and table format, respectively.

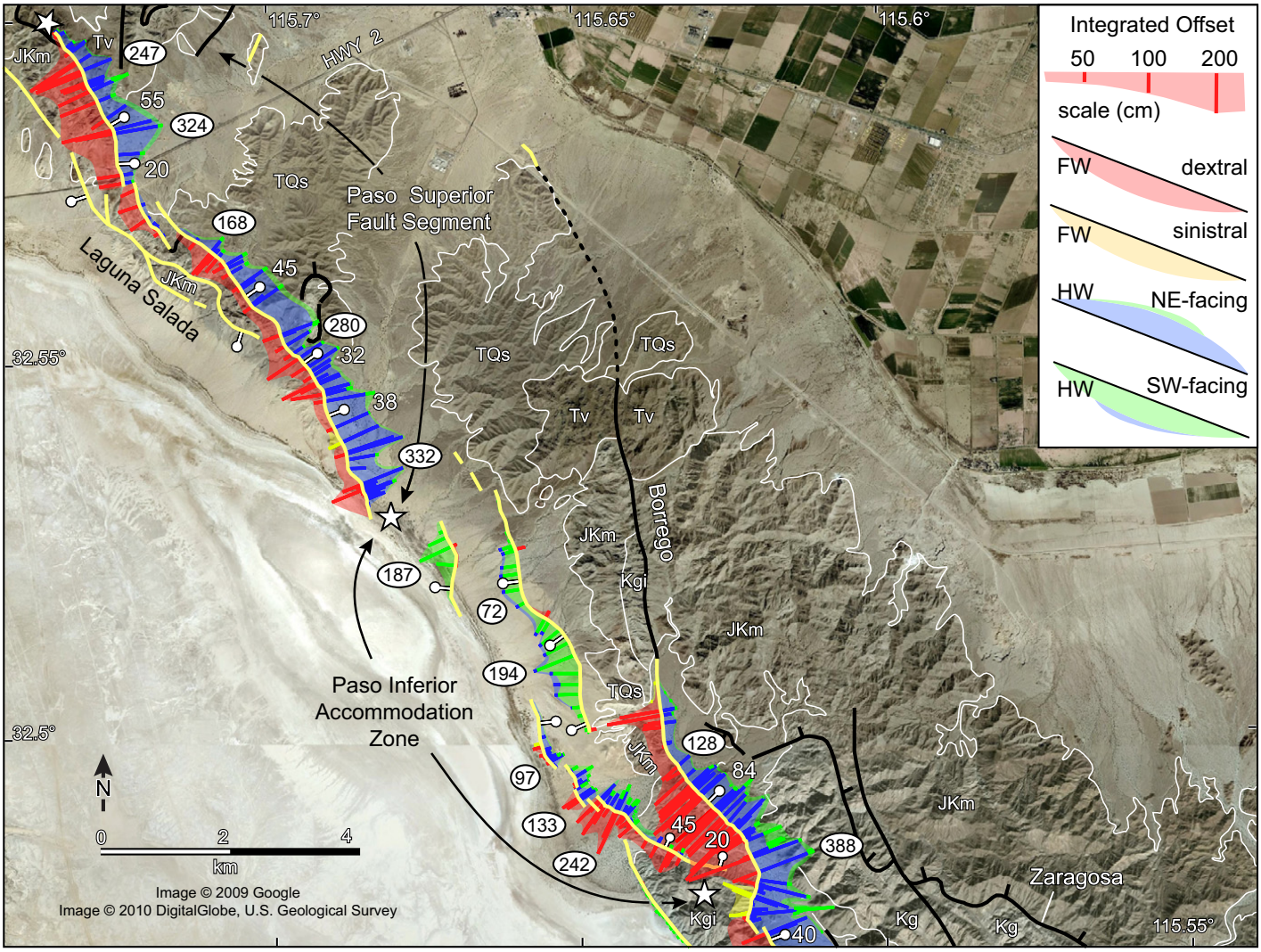

Figure 18. Geologic map of the northern Sierra domain showing schematic rupture traces (yellow lines), and distribution and magnitude of coseismic displacements measured in the field. White ellipses contain integrated total slip estimates (in centimeters) for groups of field measurements made in transects. Slip components are plotted as line symbols scaled to slip magnitude. Lateral and vertical components of slip are plotted in the footwall (FW) and hanging wall (HW), respectively. Shaded envelopes show along-strike variations in slip magnitude and extrapolate across the high and intermediate peaks in field slip data. White stars demarcate limits of the Paso Inferior accommodation zone and the Paso Superior fault segment. Unit abbreviations as in Figure 7 legend.

dominated by normal displacement that reaches a maximum of 194 cm (Fig. 18). Only minor amounts of right-lateral displacement were observed along short sections of this fault (Fig. 18). Ground cracks with as much as several centimeters of offset were observed between faults, but these were not systematically mapped throughout the accommodation zone. This subpenetrative fracturing represents the accumulation of off-fault strain, as suggested by modeling (Oskin et al., 2012).

In summary, many of the main fault strands in the Paso Inferior accommodation zone dip steeply to the west and are antithetic to the east-directed hanging-wall transport of the main faults in the Sierra Cucapah. The northern and southern extremes of the Paso Inferior accommodation zone are defined by east-rooting detachment faults, and we propose that despite the lack of continuous surface exposure, they are actually the same. Coseismic slip increases through the southern part of the accommodation zone, but then abruptly decreases as slip is transferred from the detachment to the west-dipping antithetic faults. In addition, the lateral component on many sections of west-dipping faults is relatively small. These two observations indicate that the coseismic slip did not completely propagate to the surface and that much of the missing slip may be the strike-slip component. Alternatively, the occurrence of penetrative ground cracking indicates that the missing slip may have been accommodated by penetrative off-fault deformation.

Paso Superior Fault Segment

The EMC earthquake revealed the activity of the Paso Superior detachment fault, along which rupture extends 9.5 km. Previous mapping in this area had demonstrated the existence of isolated exposures of low-angle detachments that form the base of the sedimentary basin and they were all inferred to be young, but inactive (Axen and Fletcher, 1998; Chora-Salvador, 2003;

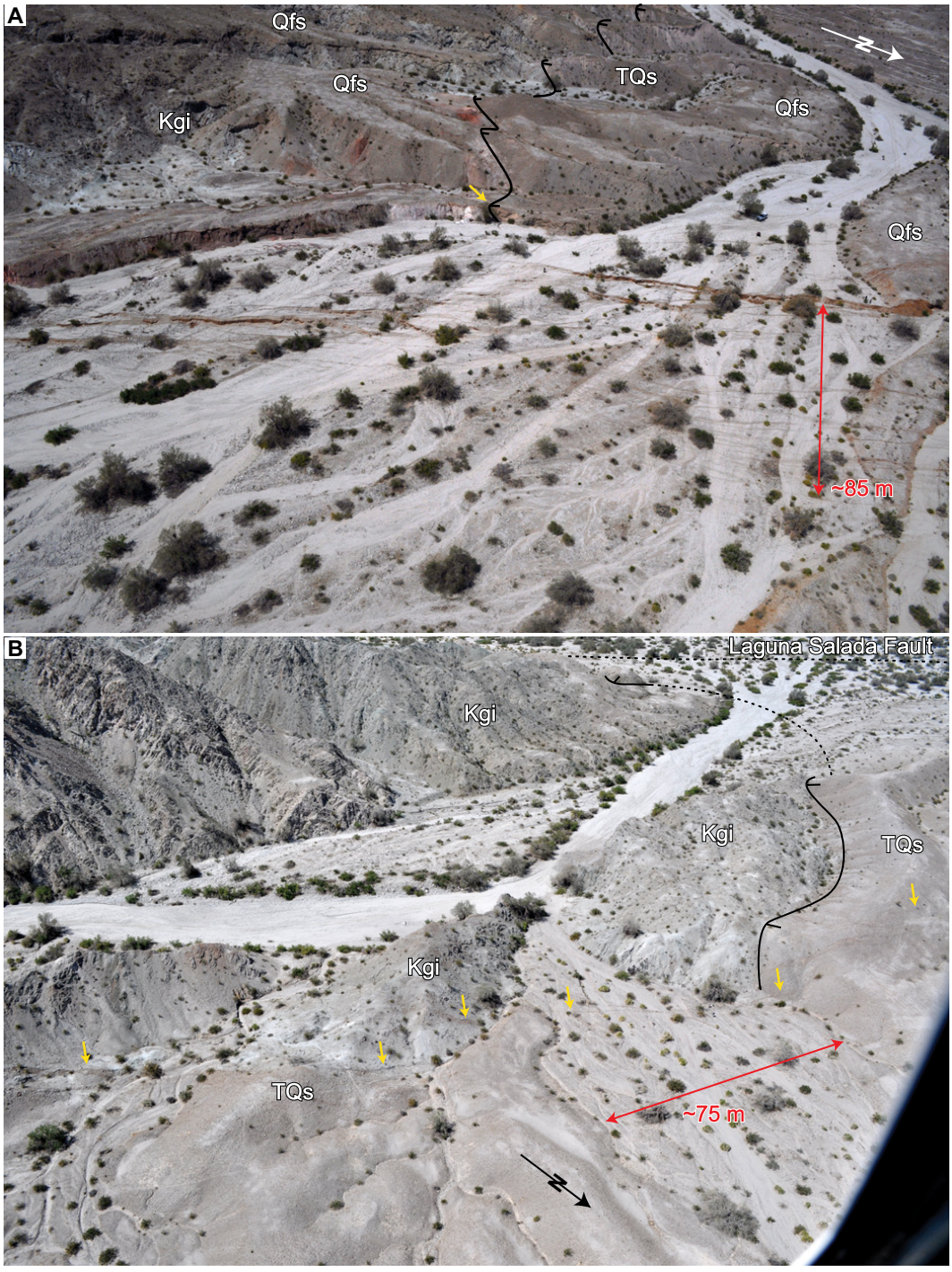

Figure 19. Field photos of structural relations and faults in the Paso Inferior accommodation zone in the Sierra domain. Unit abbreviations as in Figure 7 legend. (A) El Mayor–Cucapah (EMC) rupture forms a broad array with left-stepping principal scarps along the Borrego fault. The Borrego fault is intersected by a 20° dipping low-angle detachment in its footwall (yellow arrow). Solid black line marks the detachment fault contact and zone of chloritic gouge, breccia, and cataclasite in its footwall, which extends beyond the limits of the photo. This intersection defines the southern limit of the Paso Inferior accommodation zone. Photo azimuth is ~250°. (B) EMC rupture (yellow arrows) closely follows the contact of the same detachment fault (black line) shown in A over a short section and then diverges into the hanging wall where the detachment curves strongly toward the strike of the Laguna Salada fault (at top right of photo). Photo azimuth is ~235°. Photos taken by John M. Fletcher. See Supplemental Files 1 and 2 (see footnotes 1 and 2) for photo information in Google Earth KMZ format and Microsoft Excel table format, respectively.

Fletcher and Spelz, 2009). Not all of the known exposures of the basin-bounding detachment slipped in 2010. However, those that did rupture have a remarkably shallow inclination, as low as ~20° (Fig. 18). All sections of the Paso Superior detachment accommodate strongly oblique dextral-normal slip. Therefore, this earthquake produced the first well-documented example of a seismically active low-angle normal fault that also accommodates significant lateral offset.

The Paso Superior detachment is the structurally lowest fault in the east-directed fault array of the Sierra domain. It juxtaposes Mesozoic crystalline basement with a thick section of boulder conglomerates and gravels that make up the sedimentary basin exposed over the full width (3–5 km) of the northern Sierra Cucapah in its hanging wall (Fig. 7). The fault zone of the Paso Superior detachment reaches thicknesses of as much as 100 m and is the widest of all master faults in the Sierra domain. In addition to penetrative gouge and breccia, chloritic alteration and coherent cataclasites are common in the fault zone; this indicates that they were unroofed from deeper levels in the seismogenic crust. All of these structural characteristics suggest that the Paso Superior detachment has the most net geologic offset of any fault in the east-directed array of the Sierra Cucapah.

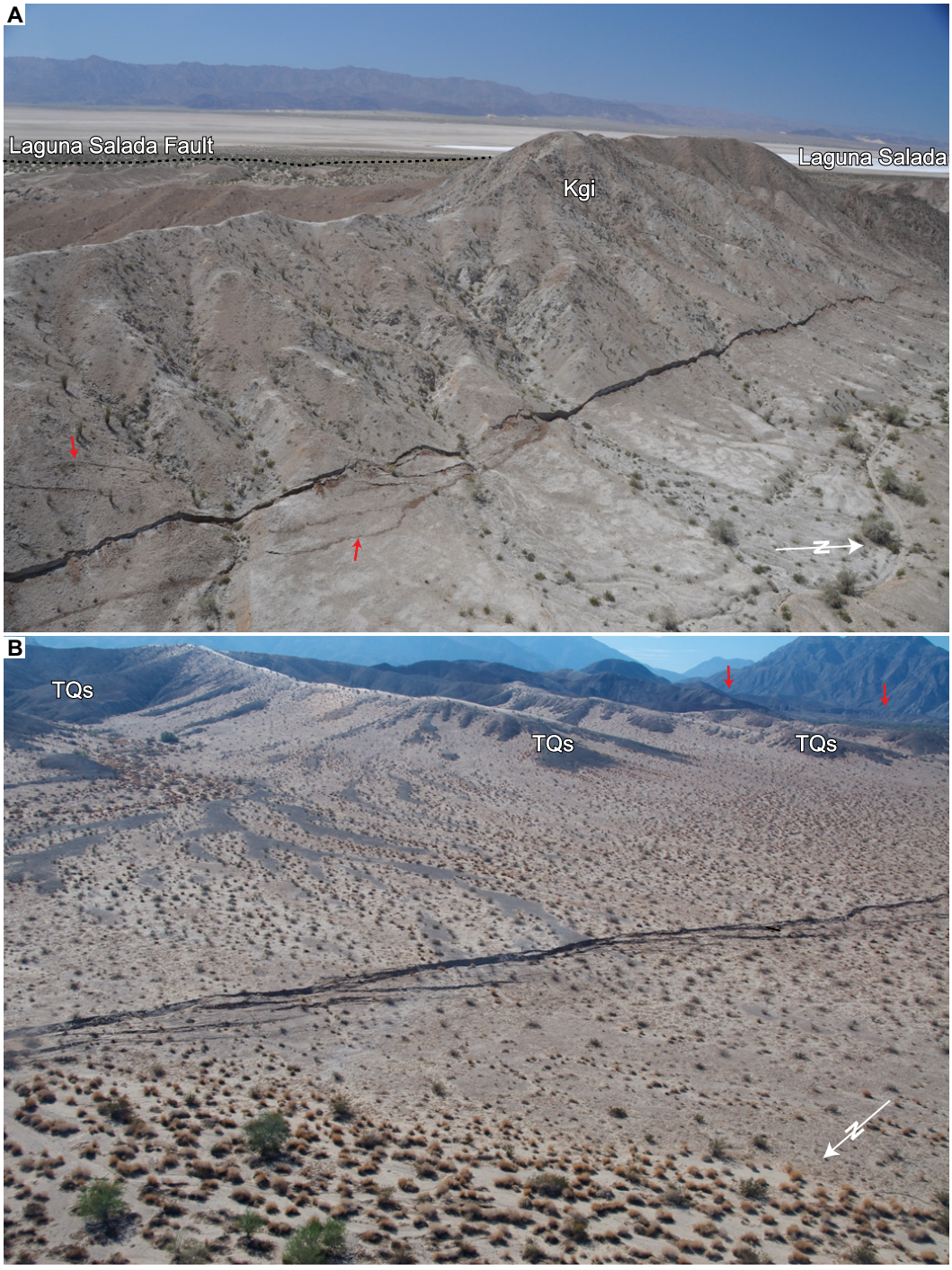

Figure 20. Field photos of El Mayor–Cucapah (EMC) rupture on faults in the Paso Inferior accommodation zone in the Sierra domain. Unit abbreviations as in Figure 7 legend. (A) Photo shows a well-defined principal scarp (length in photo is ~450 m) along the northern Borrego fault. Secondary scarps include synthetic thrust faults and oblique Riedel shears (upward- and downward-pointing arrows, respectively). The straight trace of the principal scarp reflects the subvertical dip of the Borrego fault in this section. Coseismic displacement reaches 320 cm but this is only one of several faults that have partitioned EMC rupture in the Paso Inferior accommodation zone. Photo azimuth is ~275°. (B) EMC rupture on an unnamed fault that dips steeply to the west (toward the lower right of photo). Well-defined principal scarp (length in photo is ~250 m) with left-stepping Riedel fractures. Uplifted basin fill deposits (TQs) form a series of hills in the footwall that have been recessed from the fault trace. Red arrows show the mountain front controlled by the detachment that defines the structural limit of the Paso Inferior accommodation zone in the south (see Fig. 19). Photo azimuth is ~130°. Photos taken by John M. Fletcher. See Supplemental Files 1 and File 2 (see footnotes 1 and 2) for photo information in Google Earth KMZ format and table format, respectively.

Along most of the Paso Superior detachment, the vertical component of coseismic slip is slightly greater than the right-lateral component and, in general, right-lateral slip increases toward the north (Fig. 18). Total coseismic slip reaches 332 cm and is generally >250 cm along most of the segment. However, slip diminishes slightly near a small left step in the rupture array located south of Highway 2 (Fig. 18). Offset markers include channels, ridges, alluvial deposits, and a host of anthropogenic markers such as a network of four-wheel drive roads, Highway 2, abandoned segments of Highway 2, and boundaries of military rifle ranges marked by linear rows of painted boulders (Figs. 10E, 10F, 10H).

The southern Paso Superior detachment is not exposed, but the location of the blind structure is marked by the EMC rupture array, which follows the base of a series of hills containing uplifted gravel deposits along the margin of the Laguna Salada basin (Fig. 21A). To the north, the footwall crystalline block becomes well exposed where the detachment contact steepens to 45° in a ramp section that extends ~0.3 km. Here, the structurally lowest scarps of the EMC array have the same inclination as the master fault and follow the trace of the detachment contact (Fig. 21B).

Like the Borrego fault, the Paso Superior detachment has a curvilinear trace that reflects

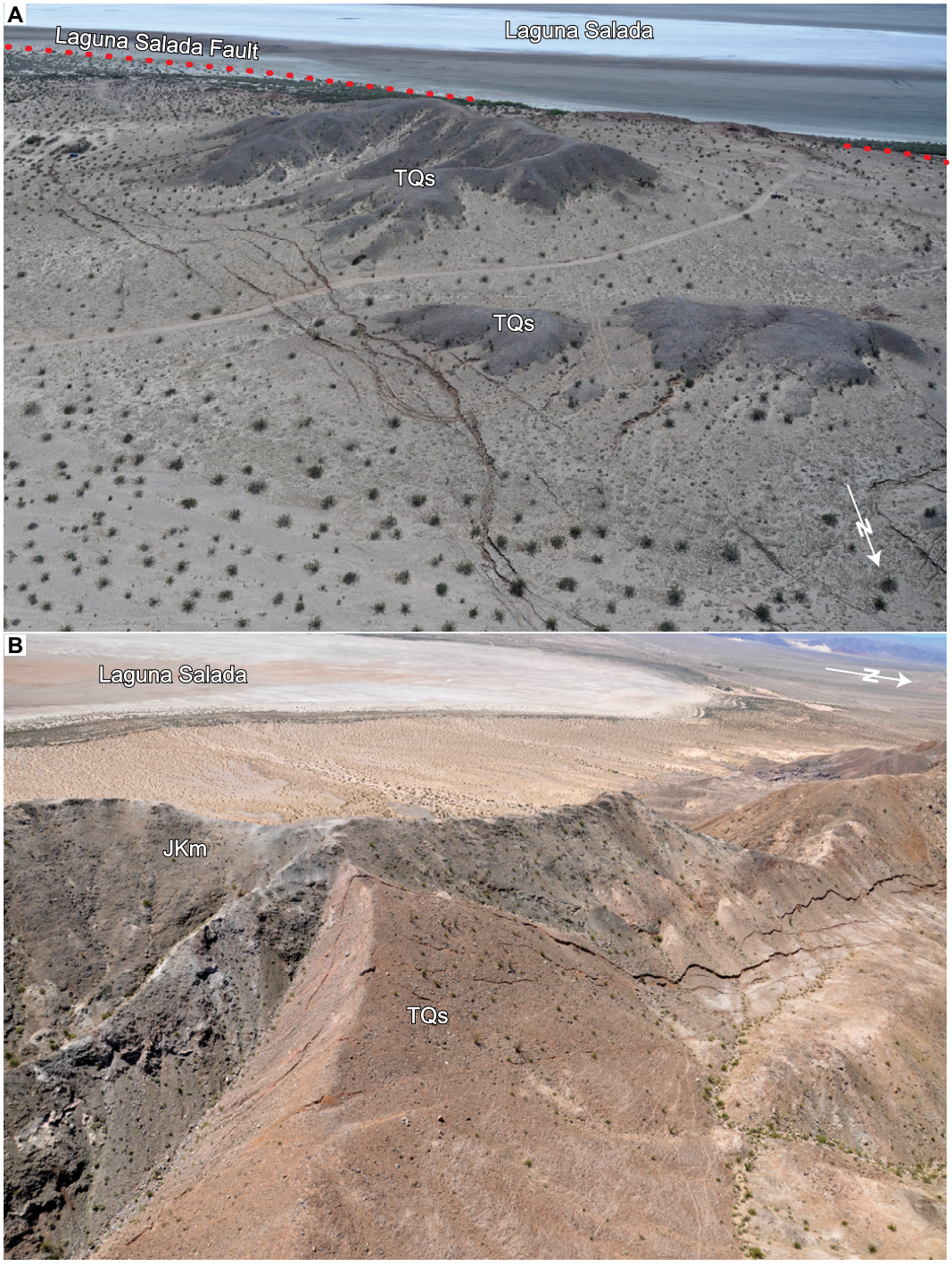

Figure 21. Field photos of the Paso Superior detachment in the Sierra domain. (A) Southernmost exposure of the scarp array associated with the Paso Superior detachment. The master fault is not exposed in this section, but the trace of the fault is defined by the eastern margin of the low hills of uplifted basin fill deposits (TQs—Pliocene–Pleistocene conglomerate). Unit abbreviations as in Figure 7 legend. Sense of east-down dip-slip displacement on the El Mayor–Cucapah (EMC) rupture is opposite to that of the west-down Laguna Salada fault, which has faster slip rates and controls the subsidence of the northern Laguna Salada basin. Photo azimuth is ~200°. (B) EMC surface rupture closely follows fault contact of the central Paso Superior detachment, which juxtaposes Mesozoic metamorphic (JKm) basement with TQs. Integrated coseismic surface rupture here has ~50 cm of lateral and ~122 cm of east-down normal slip. Dip of the basal coseismic scarp is 45°, which is slightly greater than dip of the detachment fault contact. Photo azimuth is ~265°. Photos by John M. Fletcher (A) and Kenneth W. Hudnut (B). See Supplemental Files 1 and 2 (see footnotes 1 and 2) for photo information in Google Earth KMZ format and Microsoft Excel table format, respectively.

the presence of megamullions. The EMC rupture array does not curve to conform to all of the changes in strike that define the megamullions, but instead splays into en echelon steps and shows distributed surface rupture over a width of nearly 1 km, which corresponds to the amplitude of the megamullions. Highway 2 is located near the axis of a synformal megamullion, and here the rupture array is entirely located in the hanging wall of the Paso Superior detachment, which is well exposed in a deep roadcut and dips <20° (Figs. 22A and 23). Scarps near the fault trace accommodate normal-sense dip slip, and nearly twice as much strike slip is partitioned across a 100–150-m-wide zone of cracking and minor faulting to the east (Fig. 22A).

North of Highway 2, the relief of the footwall block increases dramatically by 300 m adjacent to a second ramp in the detachment fault (Fig. 22B). This ramp is longer (~1.5 km) and steeper (55°) than the one to the south, and much of the chloritic cataclastic zone has been cut out of the footwall. However, shallowly dipping foliated cataclasite crops out on the hanging-wall side of the EMC rupture and it is clearly refractured along discrete slip surfaces; this indicates that coseismic rupture likely propagated along the gently dipping fault zone before becoming diverted along the ramp near the surface.

Figure 22. Field photos of the Paso Superior detachment in the Sierra domain. (A) El Mayor–Cucapah (EMC) scarp array reaches 800 m in width and crops out on the hanging-wall side of the detachment fault contact exposed in the roadcut of Highway 2. Some individual scarps are subparallel to the master fault trace and others are highly oblique (marked by long and short yellow arrows, respectively). The oblique fracture set has a left-stepping en echelon geometry and accommodates the dextral component of coseismic slip. Dashed line marks detachment fault contact. Photo azimuth is ~300°. Qfs—Quaternary fan surfaces and basin fill. Unit abbreviations as in Figure 7 legend. (B) EMC scarp array (yellow arrows) along a moderately dipping (55°) section, which represents an along-strike ramp on the Paso Superior detachment (black dashed line). Fault zone in the footwall is thinner and has significantly less alteration and brecciation than the low-angle sections of the detachment. TQs—Pliocene–Pleistocene conglomerate. Photos taken by John M. Fletcher. See Supplemental Files 1 and 2 (see footnotes 1 and 2) for photo information in Google Earth KMZ format and Microsoft Excel table format, respectively.

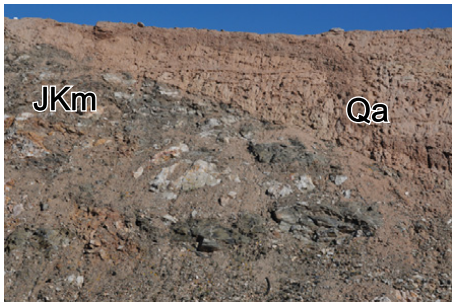

Figure 23. Fault contact of the Paso Superior detachment located in Highway 2 road cut shown in Figure 22A. The detachment fault juxtaposes Mesozoic gneissic rocks (JKm) with late Quaternary basin fill (Qa) and dips 20° in this section. Field of view ~8 m wide; photo azimuth is ~340°. Photo taken by Thomas K. Rockwell. See Supplemental Files 1 and File 2 (see footnotes 1 and 2) for photo information in Google Earth KMZ format and table format, respectively.

Primary rupture in the northernmost Sierra domain leaves the Paso Superior detachment and expands into a zone of distributed surface fractures with minor offset through the Yuha Desert domain to the north (Figs. 3 and 6). Here the Paso Superior detachment curves strongly toward the west, and is not exposed north of its intersection with the Laguna Salada fault. Most of the faulting in the Yuha Desert domain is located in the hanging wall of the north-dipping Paso Superior detachment, which likely forms the structural floor of the Yuha Desert domain (Figs. 3 and 6).

KINEMATIC ANALYSIS

In the Sierra Cucapah, the 2010 rupture propagated ~55 km through a geometrically and kinematically complex array of faults, which we have subdivided into 4 master fault segments and 2 accommodation zones (Fig. 24). On the 4 master faults, total coseismic slip typically averages more than 2 m and individual measurements that reach 3–4 m are common. In the two accommodation zones, total coseismic slip measured on discrete faults diminishes; however, this is largely due to either lack of preservation of surface faulting or distributed penetrative off-fault deformation as documented in the Puerta and Paso Inferior accommodation zones, respectively.

The Borrego fault segment is located between two stepover accommodation zones. We have defined its limits to coincide with the location where coseismic slip diverges from a single master fault and becomes partitioned onto multiple master faults, the defining characteristic of the accommodation zones in this study. Therefore, portions of the lateral limits of the 2010 rupture on the Borrego fault are classified to form part of each accommodation zone. These sections are interesting because although slip is partitioned onto multiple faults, total slip magnitudes are much higher than other parts of the accommodation zone and more similar to total slip observed in other segments where rupture is controlled by a single master fault. Therefore, we identify two transition sections on either end of the Borrego fault, which has characteristics of both an accommodation zone and a master fault segment.

The greatest coseismic slip documented on a single fault is 388 cm, which was observed on a section of the Borrego fault in the southernmost transition region of the Paso Inferior accommodation zone (Fig. 18). However, because slip in this section is partitioned on 2 different master faults, the integrated coseismic slip is >4 m (Fig. 24). Rupture sections with the least amount of coseismic slip are hard to confidently identify with the results of field slip surveys. For example, our results indicate that total slip reaches a minimum of 0.48 m in the Paso Inferior accommodation zone. However, the existence of distributed ground shattering and off-fault strain suggests that total slip is much greater and possibly has much different kinematics than recorded by offset on discrete faults. Therefore, we do not have confidence in using field slip measurements to identify sections with the smallest amount of coseismic slip due to both penetrative off-fault

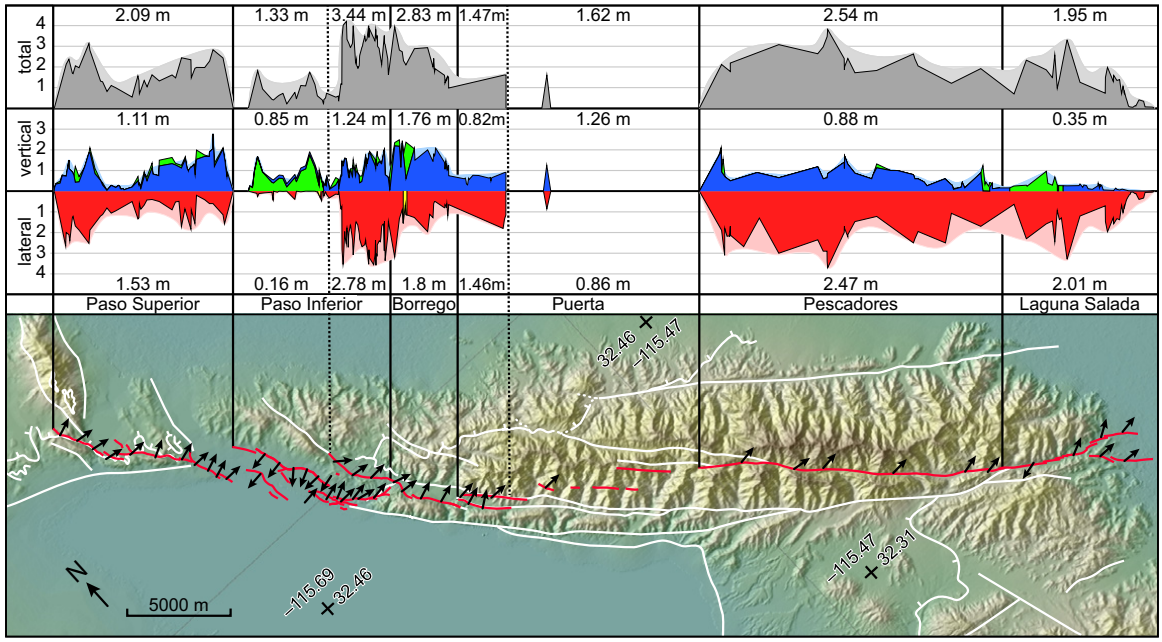

Figure 24. Distributions of lateral, vertical, and total slip documented along the main rupture segments and accommodation zones. Displacement averages for each rupture segment are shown, calculated from the shaded envelopes that reduce the radical variations between field measurements. The double curves along segments of the vertical displacement plots show the net vertical displacement (synthetic minus antithetic) plotted beneath the vertical synthetic displacement curve. The black arrows in the rupture map indicate the instantaneous extension direction (T axis) calculated for each ruptured fault section.

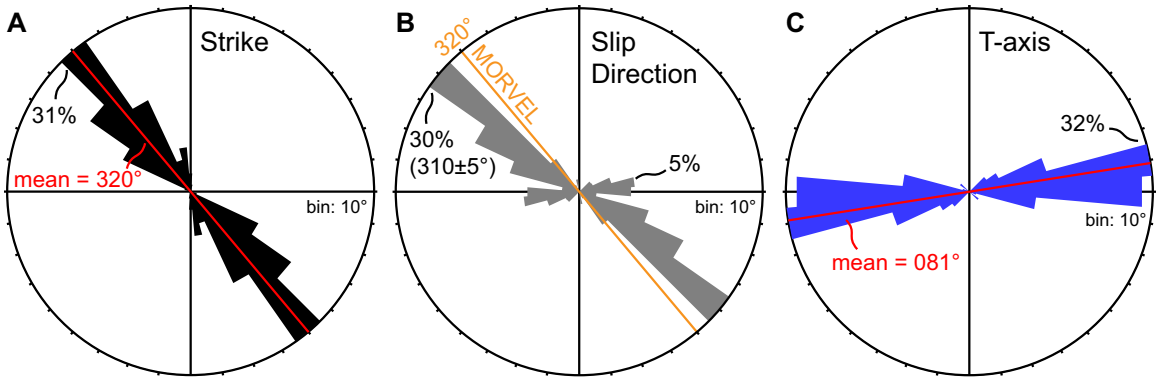

Figure 25. Rose diagrams showing length weighted distributions for rupture section strikes, slip directions, and T-axes. (A) Strike orientations span a continuous range of orientations and the dominant orientation, 31% of data, coincides with the length-weighted average. (B) Rupture section slip directions are bimodal, where 30% of the data is oriented ~10° ± 5° more westerly than the azimuth of relative plate motion (DeMets et al., 2010). (C) The derived instantaneous extension directions are uniformly oriented toward 080°, which is consistent with geodetically derived maximum extension directions for the Laguna Salada basin (Savage et al., 1994).

strain and heterogeneous distribution of geomorphic markers, which may mask important components of the total surface displacement.

The ratio of lateral to vertical coseismic slip reflects the rake of the displacement vector. In general, lateral slip exceeds vertical slip in segments where rupture is controlled by a single master fault, but variations in the ratio of lateral to vertical slip are extreme. On the Borrego fault and Paso Superior detachment, the lateral to vertical slip ratios are slightly >1, whereas the ratio rises to 3 on the Pescadores fault and is almost 8 on the Laguna Salada fault. In contrast, slip on discrete faults in the Paso Inferior accommodation zone is dominated by vertical motions and has almost no lateral component.

In order to understand the extreme variations in the ratio of lateral to vertical slip of the EMC rupture in the Sierra Cucapah, we divided the array into the 49 separate kinematic sections, which we identified based on along-strike changes in geometry and kinematics (Figs. 11, 14, and 18). We determined the geometry of each section using Bingham statistics of observed fault orientations, and calculated the rake of slip based on the ratio of lateral to vertical slip averaged over the entire section. See Supplemental File 6[6] for full documentation of the 49 geometric and kinematic rupture sections in the Sierra domain.

The strike of surface rupture weighted by section length ranges continuously from 290° to 010° with 31% of the data oriented 320° ± 5° (Fig. 25). The data are strongly skewed; most rupture sections strike with a more northerly orientation than the mode (Fig. 25). The average strike of all rupture sections weighted by length is 320°.

The projection of the vector sum of the lateral and dip-slip vectors onto a horizontal surface gives the slip direction. A rose diagram of slip directions weighted by section length demonstrates that 30% of all estimates have an azimuth of 310° ± 5° (Fig. 25). However, the slip direction data are bimodal and another smaller peak representing 5% of the data set has an azimuth of 80° ± 5°. Rupture sections with east-west–oriented slip directions are dominated by normal dip-slip kinematics. We hypothesize that in these sections, the partitioning of slip precluded the documentation of the full rupture kinematics. In general, the dominant slip direction (~310°) is oriented ~10° more westerly than the average strike (~320°) of the rupture sections, which requires oblique dextral-normal slip (Fig. 25). We note that the slip direction of ~310° is slightly oblique to the azimuth of relative plate motion, which is 320° (DeMets et al., 2010) at this latitude.

Using the fault-slip measurements and fault geometry, infinitesimal strain axes were calculated for each of the 49 rupture sections (Supplemental File 6 [see footnote 6]). The T-axis represents the principal extension direction of the infinitesimal strain ellipsoid, which is in general distinct from the least compressive principal stress ($\sigma 3$) and the direction of relative plate motion. A rose plot demonstrates that T axes are relatively uniformly oriented and have an average orientation of 081° (Fig. 25). This orientation coincides well with the principal extension direction of infinitesimal strain determined to be 080° ± 2° from a trilateration geodetic survey across the Laguna Salada basin (Savage et al., 1994).

In summary, 2010 rupture in the Sierra Cucapah shows a diverse range of geometries and kinematics. However, the relative homogeneity of overall slip azimuths and T axis orientations indicates that regional stress is likely to be the dominant factor controlling kinematics.

MECHANICAL INTERACTIONS ACROSS THE SIERRA CUCAPAH FAULT SYSTEM

The EMC earthquake demonstrated that the array of faults in the Sierra Cucapah have mechanical links that enabled the propagation of rupture through multiple faults. This study demonstrates that each fault has distinct geometry and kinematics, and that systematic along-strike variations in these parameters yield new insight into the mechanics of transtensional fault networks.

Detachment Fault Slip

In general, the east-dipping fault array in the Sierra Cucapah can be thought of as an imbricate stack or fan of faults because individual faults dip progressively less steeply at lower structural levels, from subvertical for the Laguna Salada fault to as low as 20° for the Paso Superior detachment. Many of the east-dipping faults splay to the northwest from the subvertical Laguna Salada fault, which forms the southwest boundary to the imbricate fault

[6]Supplemental File 6. Fault section geometry and EMC rupture kinematics in the Sierra domain. If you are viewing the PDF of this paper or reading it offline, please visit http://dx.doi.org/10.1130/GES00933.S6 or the full text article on www.gsapubs.org to view Supplemental File 6.

system. The northernmost and structurally lowest rupture segment is controlled by the Paso Superior detachment, with a strike length of at least 9.5 km. Therefore, the EMC earthquake is the first modern rupture with dominantly strike-slip kinematics that is known to have occurred, in part, on a low-angle detachment fault.

Assembly of Individual Faults into a Single Rupture

Rupture through the Sierra Cucapah defines a path with an overall arcuate shape, and fault strikes vary systematically from 290° in the south to 340° in the north. However, the overall rupture is also characterized by a left-stepping en echelon geometry at scales that range from the macroscopic accommodation zones that span distances to 10 km (e.g., Puerta and Paso Inferior accommodation zones) to mesoscopic arrays with centimeter-scale fracture spacing. Therefore, individual fractures and rupture faults are oriented with a strike that is in general more northerly than the overall trend of the rupture, which can be approximated by a straight line with an azimuth of 312°. Although such an orientation is consistent with the simplified, geophysically defined rupture geometry (S. Wei et al., 2011), our data demonstrate that tectonic stress activated slip on planes with a wide spectrum of orientations and, in general, seems to have favored planes with a more northerly strike.

The en echelon steps in the path of the rupture not only allowed the rupture to have a more westerly strike than individual fractures and rupture segments, but they also formed the dominant mechanism for transferring slip to structurally lower master faults in the imbricate stack. In contrast to the ubiquitous left-stepping arrays, right stepping arrays are virtually absent and are only manifested in the macroscopic curvature observed at the lateral limits of the rupture in the Yuha Desert and Delta domains. The most likely mechanical explanation for the left-stepping arrays is that they accommodate dextral shear, which is the dominant kinematic component of the 2010 rupture. It is also likely that the left-stepping geometry and northward-curving fault tips reflect the obliquity between the optimum fracture orientation (i.e., one that maximizes the ratio between shear and normal stress) and the more westerly overall trend of the rupture.

TECTONIC STRESS AND FAULTING IN THE BIG BEND DOMAIN

Historic earthquakes in the Big Bend domain commonly involve multiple faults that link together in complex and often unanticipated ways (Fig. 2). For example, the three most recent large earthquakes in southern California and northern Baja California (1992 Landers, 1999 Hector Mine, 2010 EMC) all involved multiple faults with only parts of some faults rupturing along with others (Fig. 2). In Rockwell et al. (2000), it was demonstrated that the fault system behavior of the Landers earthquake is just one way that these individual faults can be linked and successive ruptures do not follow the same paths. The close proximity of the Landers (M_w 7.3) and Hector Mine (M_w 7.1) earthquakes surprised experts and provided new understanding for how large earthquakes cluster in space and time (Freed and Lin, 2001; Felzer et al., 2002; Oskin et al., 2008). Paleoseismic studies on faults that ruptured in the Landers earthquake confirmed the clustering hypothesis and indicated bursts of rupture events over short punctuated time periods followed by long quiescent intervals (5 k.y.) of strain buildup (Rockwell et al., 2000).

Nearly twice as many large historical earthquakes in the Big Bend domain are located on fault systems that are distinct from the dominant strands that have accommodated the largest finite slip (i.e., San Andreas, Imperial, and Cerro Prieto faults; Fig. 2). Large earthquakes in the Big Bend domain commonly nucleate in zones of diffuse strain such as the eastern California shear zone and the Sierra Cucapah terrane, which is sandwiched between fault systems that likely have an order of magnitude faster slip rates (Fig. 3). Many of the most active fault strands within the Big Bend domain, such as the San Miguel, Vallecitos and San Jacinto faults, are very young with low magnitudes of finite offset and have formed only within the past 1–2 m.y. (Fig. 2; Janecke et al., 2011; Dorsey et al., 2012; McGill et al., 2013). In contrast, the southern San Andreas fault has been ominously quiet for more than 300 yr (Fumal et al., 2002; Philibosian et al., 2011), and late Quaternary slip rates decrease by more than a factor of two south of its intersection with the San Jacinto fault (McGill et al., 2013). Although the southern San Andreas fault is considered overdue for a large earthquake, a lot of plate boundary slip has been taking place on the San Jacinto fault (Janecke et al., 2011) as well as on other faults with more favorable orientations (e.g., Nur et al., 1993; Du and Aydin, 1996). These issues underscore the challenge of accurately forecasting future earthquakes and there is general consensus that even in hindsight, many of the historic earthquakes in the Big Bend domain remain a surprise.

Longer term patterns of faulting in the Big Bend domain show even more complexity than is exhibited by historical ruptures and the large-scale kinematics of faulting show extreme spatial variations. Plate margin shearing from the Gulf of California bifurcates in the middle of the Big Bend domain and becomes partitioned into the San Andreas and Eastern California fault systems (Fig. 1; Faulds and Henry, 2008). In addition, the fundamental change in character of plate margin shearing from transtension in the Gulf of California to transpression on the San Andreas fault system also occurs in the middle of the Big Bend domain near the Salton Sea (Fig. 1).

Several key observations strongly indicate that both the redistribution of plate margin shearing and the reversal in the character of fault-normal strain reflects the influence of the ongoing collapse of the Great Basin. First, fault-perpendicular shortening is not restricted to the restraining bend segments of faults with more westerly strikes, but rather is observed along nearly the entire length (>1000 km) of the San Andreas fault system, and the orientation of subhorizontal maximum compressive stress changes systematically as fault traces become deflected around the southwest margin of the Great Basin (Townend and Zoback, 2004; Yang and Hauksson, 2013). The maximum horizontal compressive stress rotates more than fault strike and becomes more orthogonal to the San Andreas fault in central California north of the Big Bend domain (Fig. 1; Townend and Zoback, 2004). Second, along the southern margin of the Great Basin, Quaternary thrust faults and folds are distributed broadly throughout the Mojave block and accommodate regional north-south shortening and crustal thickening (Bartley et al., 1990). Geodynamic modeling has shown that, due to high mean elevation, heat flow, and anomalously buoyant mantle, the Great Basin has excess gravitational potential energy, which drives internal extension and causes the terrain to push outward on all of its margins (Jones et al., 1996; Flesch et al., 2000). Although some propose that extension in the Great Basin simply tracks the westward drift of the Pacific plate (Dixon et al., 1996; Wernicke and Snow, 1998), crustal shortening around its margins requires internal extension to be multidirectional and occurs at rates that exceed relative plate separation. Therefore, it is likely that the left-stepping deflection of the Big Bend has amplified through time due to bulging of the continental margin adjacent to the Great Basin. A third key observation is that along the southern limit of the Big Bend domain, faults with more westerly strikes such as the Agua Blanca fault accommodate transtensional shearing despite having the same geometry as restraining bend segments of the San Andreas farther north (Callihan, 2010; Springer, 2010; Wetmore et al., 2012). This demonstrates that the horizontal deviatoric compres-

sion around the margins of the Great Basin is not transmitted all the way across the Big Bend domain and that restraining bend kinematics are perhaps not as important as gravitational potential energy gradients for inverting the sense of fault-normal strain. However, both gravitational potential energy gradients and the rerouting of plate margin shearing require extreme spatial variations in the orientation and relative magnitudes of principal stress. These geodynamic processes operate in addition to relative plate motion, which helps to explain why faults that ruptured in the Landers earthquake have a much more northerly strike (to 40°; Hauksson, 1994) than those of the EMC event, even though both events are dominated by strike slip.

Perhaps the most important factor controlling the assembly of complex multifault ruptures in the Big Bend domain is the three-dimensional strain produced in both transtensional and transpressional shear zones. Shear zones that expand or contract perpendicular to their margins produce three-dimensional strain that is constrictional or flattening, respectively. In contrast, slip on a single fault accommodates only two-dimensional plane strain. Therefore multiple faults, typically more than four sets with distinct orientations and kinematics, are required to accommodate three-dimensional strain (Reches, 1983; Yin and Ranalli, 1992; Unruh and Lettis, 1998; Nieto-Samaniego and Alaniz-Alvarez, 1997). In the EMC surface rupture, we observe that slip was activated on faults with a wide spectrum of orientations and the rake of slip is directly controlled by fault strike. A geometrically and kinematically complex network of faults such as this is in fact required to produce the three-dimensional constrictional strain of transtensional shearing. In addition, because slip is commonly partitioned into multiple sets of faults that occur in the same rock volume, we hypothesize that different sets may be activated in different earthquakes. Therefore, the assembly of fault segments that link together to produce a large earthquake need not be replicated in consecutive ruptures.

CONCLUSIONS

The M_w 7.1 EMC of 4 April 2010 produced the most complex rupture ever documented on the Pacific–North American plate margin. Mapping and structural analysis of discrete surface rupture and distributed ground failure is consistent with rupture initiating on a north-striking fault and then propagating bilaterally to the northwest and southeast. Slip cascaded through a network of at least seven distinct master faults, which have a large range of diversity in geometry and kinematics. Fault segments that have end-member kinematics of either pure normal or dextral slip are relatively rare compared to those with oblique-slip kinematics and thus the overall slip direction is more westerly than the average trend (312°) of the rupture. Low-angle detachments control large segments of the surface rupture and played an important role in transferring slip through the fault network. Complex multifault ruptures that deviate from the from the direction of relative plate motion are common in the Big Bend domain due to the redistribution of plate margin shearing and the three-dimensional strain that is an inherent aspect of transtensional and transpressional shear zones.

ACKNOWLEDGMENTS

This work was financed by CONACYT (Consejo Nacional de Ciencia y Tecnología) grant 81463, SCEC (Southern California Earthquake Center) grant 1697, and National Science Foundation grant EAR-0529922; the GEER (Geotechnical Extreme Events Reconnaissance) Foundation provided funding for initial field work. S. Leprince was supported in part by the Keck Institute for Space Studies and by the Gordon and Betty Moore Foundation. Part of this study was sponsored by the National Aeronautics and Space Administration (NASA) Earth Surface and Interior focus area and performed at the Jet Propulsion Laboratory, California Institute of Technology, under contract with NASA. Enlightening discussions with Paul Wetmore and Francisco Suarez helped refine ideas about tectonics of the Big Bend domain and the kinematics of faulting in the Colorado River delta, respectively. We thank John Galetzka, Kate Scharer, David Bowman, Roman Manjarrez, and Maria Oturno for help with field work. We also thank Jose Mojarro, Sergio Arregui, and Luis Gradilla for technical support.

APPENDIX 1. MEASUREMENT TRANSECT ESTIMATES

Methods for integrating displacement from multiple measurements are described here. Rupture in the Sierra Cucapah occurred across an array of multistrand faults. Measurement transects oriented at a high angle to the array crossed as many as 19 individual scarps and fractures of varying orientations. Total coseismic slip was calculated by a vector summation of the three components of slip (lateral, heave, and vertical) measured in each scarp. The strike of every scarp was directly measured in the field and/or using their traces in map view, but in some cases scarp dip could not be measured because of a lack of three-dimensional exposure.

Therefore, in order to calculate the heave component of slip, a dip of 65° in the direction of vertical downdropping was assumed. The three components of slip in the scarp reference frame were converted to spatial coordinates: north, east, and down for the vector summation. The final vector summation was converted back to slip components relative to the local orientation of the master fault. Because geomorphic markers of vertical offset were the most abundant, this component of slip is the most accurate. In contrast, because it was not possible to directly measure the dip of every scarp in any given transect, the heave component of integrated slip is the least reliable. For this reason we do not report integrated heave calculated by vector summation. Instead, integrated heave is calculated using the integrated vertical displacement and the dip of the master fault, both of which are more robust measurements.

There are cases where the master fault dip could not be directly measured near a given transect due to a lack of exposure. In these cases we employed two conventions for approximating master fault dip. The first was to assume the master fault to have the same dip as that of the shallowest scarp-forming fracture measured near the transect. Field relationships demonstrate that scarp-forming faults are systematically inclined at higher angles than the master fault along which they propagated, and the disparity in inclination increases as the dip of the master fault decreases. Therefore, the shallowest dipping scarp is considered to be a maximum estimate of the true dip of the master fault. In rare cases it was not possible to systematically measure the inclination of individual scarps because of a lack of topographic relief to make three-point determinations. In these cases, the second convention was to assume the master fault dip based on structural context and known along-strike characteristics of the fault zone. Entries with assumed dips are clearly marked in the "Dip Source" field in Supplemental File 4 (see footnote 4).

Transects were designed to be as comprehensive as possible, but in some cases not all components of slip could be measured on all individual scarps due to the heterogeneous distribution of slip markers and/or incomplete exposure of the scarps. Therefore, some transects only integrate the vertical component and other transects only integrate the lateral components. Scarps with <5 cm of offset were not systematically measured by all geologists who contributed to the data slip database. Therefore, our measurements of total coseismic slip represent minimum estimates.

REFERENCES CITED

Abrahamson, N.A., and Somerville, P.G., 1996, Effects of the hanging wall and footwall on ground motions recorded during the Northridge earthquake: Seismological Society of America Bulletin, v. 86, no. 1B, p. S93–S99.

Alvarez-Rosales, J., Camacho-Hernandez, J.M., Gallardo-Federico, V.I., Macias-Valdez, G., and Herrera-Carrillo, D., 2012, Preliminary geologic features of the new geothermal zone Cucapah at the Mexicali Valley, BC, Mexico: Revista Mexicana de Geoenergia, v. 25, p. 21–27.

Anderson, J.G., and Bodin, P., 1987, Earthquake recurrence models and historical seismicity in the Mexicali-Imperial Valley: Seismological Society of America Bulletin, v. 77, no. 2, p. 562–578.

Argus, D.F., and Gordon, R.G., 2001, Present tectonic motion across the Coast Ranges and San Andreas fault system in central California: Geological Society of America Bulletin, v. 113, p. 1580–1592, doi:10.1130/0016-7606(2001)113<1580:PTMATC>2.0.CO;2.

Armstrong, P.A., Perez, R., Owen, L.A., and Finkel, R.C., 2010, Timing and controls on late Quaternary landscape development along the eastern Sierra El Mayor range front in northern Baja California, Mexico: Geomorphology, v. 114, p. 415–430, doi:10.1016/j.geomorph.2009.08.005.

Axen, G.J., 2007, Research focus: Significance of large-displacement, low-angle normal faults: Geology, v. 35, p. 287–288, doi:10.1130/0091-7613(2007)35[287:RFSOLL]2.0.CO;2.

Axen, G.J., and Fletcher, J.M., 1998, Late Miocene–Pleistocene extensional faulting, northern Gulf of California, Mexico and Salton Trough, California: International Geology Review, v. 40, p. 217–244, doi:10.1080/00206819809465207.

Axen, G.J., Fletcher, J.M., Cowgill, E., Murphy, M., Kapp, P., MacMillan, I., Ramos-Velazquez, E., and Aranda-Gomez, J., 1999, Range-front fault scarps of the Sierra El Mayor, Baja California: Formed above an active low-

angle normal fault?: Geology, v. 27, p. 247–250, doi: 10.1130/0091-7613(1999)027<0247:RFFSOT>2.3.CO;2.

Barnard, F.L., 1968, Structural geology of the Sierra de los Cucapas, northeastern Baja California, Mexico, and Imperial County, California [Ph.D. thesis]: Boulder, Colorado, University of Colorado, 157 p.

Bartley, J.M., Glazner, A.F., and Schermer, E.R., 1990, North-south contraction of the Mojave block and strike-slip tectonics in southern California: Science, v. 248, no. 4961, p. 1398–1401, doi:10.1126/science.248.4961.1398.

Bennett, R.A., Rodi, W., and Reilinger, R.E., 1996, Global positioning system constraints on fault slip rates in southern California and northern Baja, Mexico: Journal of Geophysical Research, v. 101, no. B10, p. 21943–21960, doi:10.1029/96JB02488.

Biehler, S., Kovach, R.L., and Allen, C., 1964, Geophysical framework of northern end of Gulf of California structural province, *in* van Andel, T., and Shore, G.G., Jr., eds., Marine geology of the Gulf of California: A symposium: American Association of Petroleum Geologists Memoir 3, p. 126–143.

Callihan, S., 2010, Constraining the geometry and evolution of the Maneadero Basin, Baja California, Mexico [M.S. thesis]: Tampa, University of South Florida, 67 p.

Chanes-Martinez, J.J., 2012, Características estructurales y sismoestratigráficas en un sector del delta del Río Colorado, noroeste de México, a partir de sísmica de reflexión [M.S. thesis]: Ensenada, Baja California, Centro de Investigacion Cientifica y de Educacion Superior de Ensenada (CICESE), 115 p.

Chora-Salvador, J.M., 2003, Analisis cinematico de fallas neogenicas normales de alto y bajo angulo en la Sierra Cucapa, Baja California, Mexico [M.S. thesis]: Ensenada, Baja California, Centro de Investigacion Cientifica y de Educacion Superior de Ensenada (CICESE), 107 p.

Cichanski, M., 2000, Low-angle, range-flank faults in the Panamint, Inyo, and Slate ranges, California: Implications for recent tectonics of the Death Valley region: Geological Society of America Bulletin, v. 112, p. 871–883, doi:10.1130/0016-7606(2000)112<871:LRFITP>2.0.CO;2.

Cortes-Arroyo, O.J., 2011, Perfil magnetotelúrico a través de una zona de deformación activa en el norte de Baja California [M.S. thesis]: Ensenada, Baja California, Centro de Investigacion Cientifica y de Educacion Superior de Ensenada (CICESE), 177 p.

DeMets, C., Gordon, R.G., and Argus, D.F., 2010, Geologically current plate motions: Geophysical Journal International, v. 181, p. 1–80, doi:10.1111/j.1365-246X.2009.04491.x.

Dixon, T.H., Mao, A., and Stein, S., 1996, How rigid is the stable interior of the North American plate?: Geophysical Research Letters, v. 23, no. 21, p. 3035–3038, doi:10.1029/96GL02820.

Dixon, T., Farina, F., DeMets, C., Suarez-Vidal, F., Fletcher, J., Marquez-Azua, B., Miller, M., Sanchez, O., and Umhoefer, P., 2000, New kinematic models for Pacific–North America motion from 3 Ma to present, II: Evidence for a Baja California shear zone: Geophysical Research Letters, v. 27, no. 23, p. 3961–3964, doi:10.1029/2000GL008529.

Dorsey, R.J., 2010, Sedimentation and crustal recycling along an active oblique-rift margin: Salton Trough and northern Gulf of California: Geology, v. 38, p. 443–446, doi:10.1130/G30698.1.

Dorsey, R.J., Axen, G.J., Peryam, T.C., and Kairouz, M.E., 2012, Initiation of the Southern Elsinore fault at ~1.2 Ma: Evidence from the Fish Creek–Vallecito Basin, southern California: Tectonics, v. 31, no. 2, doi:10.1029/2011TC003009.

Du, Y., and Aydin, A., 1996, Is the San Andreas big bend responsible for the Landers earthquake and the eastern California shear zone?: Geology, v. 24, p. 219–222, doi:10.1130/0091-7613(1996)024<0219:ITSABB>2.3.CO;2.

Faulds, J.E., and Henry, C.D., 2008, Tectonic influences on the spatial and temporal evolution of the Walker Lane: An incipient transform fault along the evolving Pacific–North American plate boundary, *in* Spencer, J.E., and Titley, S.R., eds., Ores and orogenesis: Circum-Pacific tectonics, geologic evolution, and ore deposits: Arizona Geological Society Digest, v. 22, p. 437–470.

Felzer, K.R., Becker, T.W., Abercrombie, R.E., Ekström, G., and Rice, J.R., 2002, Triggering of the 1999 MW 7.1 Hector Mine earthquake by aftershocks of the 1992 MW 7.3 Landers earthquake: Journal of Geophysical Research, v. 107, no. B9, doi:10.1029/2001JB000911.

Ferrill, D.A., Stamatakos, J.A., and Sims, D., 1999, Normal fault corrugation: implications for growth and seismicity of active normal faults: Journal of Structural Geology, v. 21, p. 1027–1038, doi:10.1016/S0191-8141(99)00017-6.

Flesch, L.M., Holt, W.E., Haines, A.J., and Shen-Tu, B., 2000, Dynamics of the Pacific–North American plate boundary in the western United States: Science, v. 287, no. 5454, p. 834–836, doi:10.1126/science.287.5454.834.

Fletcher, J.M., and Spelz, R.M., 2009, Patterns of Quaternary deformation and rupture propagation associated with an active low-angle normal fault, Laguna Salada, Mexico: Evidence of a rolling hinge?: Geosphere, v. 5, p. 385–407, doi:10.1130/GES00206.1.

Fletcher, J.M., Grove, M., Kimbrough, D., Lovera, O., and Gehrels, G.E., 2007, Ridge-trench interactions and the Neogene tectonic evolution of the Magdalena shelf and southern Gulf of California: Insights from detrital zircon U-Pb ages from the Magdalena fan and adjacent areas: Geological Society of America Bulletin, v. 119, p. 1313–1336, doi:10.1130/B26067.1.

Freed, A.M., and Lin, J., 2001, Delayed triggering of the 1999 Hector Mine earthquake by viscoelastic stress transfer: Nature, v. 411, no. 6834, p. 180–183, doi:10.1038/35075548.

Freymueller, J.T., Murray, M.H., Segall, P., and Castillo, D., 1999, Kinematics of the Pacific–North America plate boundary zone, northern California: Journal of Geophysical Research, v. 104, no. B4, p. 7419–7441, doi:10.1029/1998JB900118.

Fumal, T.E., Weldon, R.J., Biasi, G.P., Dawson, T.E., Seitz, G.G., Frost, W.T., and Schwartz, D.P., 2002, Evidence for large earthquakes on the San Andreas fault at the Wrightwood, California, paleoseismic site: AD 500 to present: Seismological Society of America Bulletin, v. 92, p. 2726–2760, doi:10.1785/0120000608.

Genrich, J.F., Bock, Y., and Mason, R.G., 1997, Crustal deformation across the Imperial fault: Results from kinematic GPS surveys and trilateration of a densely spaced, small-aperture network: Journal of Geophysical Research, v. 102, no. B3, p. 4985–5004, doi:10.1029/96JB02854.

Guccione, M.J., Van Arsdale, R.B., and Hehr, L.H., 2000, Origin and age of the Manila high and associated Big Lake "sunklands" in the New Madrid seismic zone, northeastern Arkansas: Geological Society of America Bulletin, v. 112, p. 579–590, doi:10.1130/0016-7606(2000)112<579:OAAOTM>2.0.CO;2.

Hauksson, E., 1994, State of stress from focal mechanisms before and after the 1992 Landers earthquake sequence: Seismological Society of America Bulletin, v. 84, p. 917–934.

Hauksson, E., Stock, J., Hutton, K., Yang, W., Vidal-Villegas, J.A., and Kanamori, H., 2010, The 2010 M_w 7.2 El Mayor–Cucapah earthquake sequence, Baja California, Mexico and southernmost California, USA: Active seismotectonics along the Mexican Pacific margin: Pure and Applied Geophysics, v. 168, p. 1255–1277, doi:10.1007/s00024-010-0209-7.

Heidbach, O., Tingay, M., Barth, A., Reinecker, J., and Kurfeß, D., 2008, The World Stress Map database release 2008: http://www.world-stress-map.org, doi:10.1594/GFZ.WSM.Rel2008.

Hernandez, A.P., Fletcher, J.M., Spelz, R.M., Rockwell, T.K., and Teran, O.J., 2013, Paleoseismology of the imbricate fault array in the Sierra Cucapah, northern Baja California, Mexico: Proceedings, American Geophysical Union Meeting of the Americas, abs.T42A–04.

Hill, M.L., and Dibblee, T.W., 1953, San Andreas, Garlock, and Big Pine faults, California: A study of the character, history, and tectonic significance of their displacements: Geological Society of America Bulletin, v. 64, p. 443–458, doi:10.1130/0016-7606(1953)64[443:SAGABP]2.0.CO;2.

Hough, S.E., and Elliot, A., 2004, Revisiting the 23 February 1892 Laguna Salada earthquake: Seismological Society of America Bulletin, v. 94, p. 1571–1578, doi:10.1785/012003244.

Hudnut, K., Seeber, L., Rockwell, T., Goodmacher, J., Klinger, R., Lindvall, S., and McElwain, R., 1989, Surface ruptures on cross-faults in the 24 November 1987 Superstition Hills, California, earthquake sequence: Seismological Society of America Bulletin, v. 79, p. 282–296.

Hutton, K., Woessner, J., and Hauksson, E., 2010, Earthquake monitoring in southern California for seventy-seven years (1932–2008): Seismological Society of America Bulletin, v. 100, no. 2, p. 423–446, doi:10.1785/0120090130.

Janecke, S.U., Dorsey, R.J., Forand, D., Steely, A.N., Kirby, S.M., Lutz, A.T., Housen, B.A., Belgarde, B., Langenheim, V.E., and Rittenour, T.M., 2011, High geologic slip rates since early Pleistocene initiation of the San Jacinto and San Felipe fault zones in the San Andreas fault system: Southern California, USA: Geological Society of America Special Paper 475, 48 p., doi:10.1130/2010.2475.

Jones, C.H., Unruh, J.R., and Sonder, L.J., 1996, The role of gravitational potential energy in active deformation in the southwestern United States: Nature, v. 381, p. 37, doi:10.1038/381037a0.

Kim, Y., Peacock, D.C.P., and Sanderson, D.J., 2004, Fault damage zones: Journal of Structural Geology, v. 26, p. 503–517, doi:10.1016/j.jsg.2003.08.002.

Kovach, R.L., Allen, C.R., and Press, F., 1962, Geophysical investigation in the Colorado River Delta region: Journal of Geophysical Research, v. 67, p. 2845–2871, doi:10.1029/JZ067i007p02845.

Lira-Herrera, H., 2005, Actualización del modelo geológico conceptual de yacimiento geotérmico de Cerro Prieto: B.C.: Geotermia, v. 18, p. 37–46.

Ma, S., and Beroza, G.C., 2008, Rupture dynamics on a bimaterial interface for dipping faults: Seismological Society of America Bulletin, v. 98, p. 1642–1658, doi:10.1785/0120070201.

McGill, S.F., Owen, L.A., Weldon, R.J., and Kendrick, K.J., 2013, Latest Pleistocene and Holocene slip rate for the San Bernardino strand of the San Andreas fault, Plunge Creek, southern California: Implications for strain partitioning within the southern San Andreas fault system for the last 35 k.y: Geological Society of America Bulletin, v. 125, p. 48–72, doi:10.1130/B30647.1.

Morton, N., Girty, G.H., and Rockwell, T.K., 2012, Fault zone architecture of the San Jacinto fault zone in Horse Canyon, southern California: A model for focused post-seismic fluid flow and heat transfer in the shallow crust: Earth and Planetary Science Letters, v. 329–330, p. 71–83, doi:10.1016/j.epsl.2012.02.013.

Muehlberger, W.R., 1996, Tectonic map of North America: Tulsa, Oklahoma, American Association of Petroleum Geologists, scale 1:5,000,000.

Mueller, K.J., and Rockwell, T.K., 1991, Late Quaternary structural evolution of the western margin of the Sierra Cucapa, northern Baja California, *in* Dauphine, J.P., and Simoneit, B.R.T., eds., The Gulf and Peninsular Province of the Californias: American Association of Petroleum Geologists Memoir 47, p. 249–260.

Mueller, K.J., and Rockwell, T.K., 1995, Late Quaternary activity of the Laguna Salada fault in northern Baja California, Mexico: Geological Society of America Bulletin, v. 107, p. 8–18, doi:10.1130/0016-7606(1995)107<0008:LQAOTL>2.3.CO;2.

Nelson, S.M., Fielding, E.J., Zamora-Arroyo, F., and Flessa, K., 2013, Delta dynamics: Effects of a major earthquake, tides, and river flows on Ciénega de Santa Clara and the Colorado River Delta, Mexico: Ecological Engineering, v. 59, p. 144–156, doi:10.1016/j.ecoleng.2012.09.004.

Nieto-Samaniego, A.F., and Alaniz-Alvarez, S.A., 1997, Origin and tectonic interpretation of multiple fault patterns: Tectonophysics, v. 270, no. 3, p. 197–206, doi:10.1016/S0040-1951(96)00216-8.

Nur, A., Ron, H., and Beroza, G.C., 1993, The nature of the Landers-Mojave earthquake line: Science, v. 261, no. 5118, p. 201–203, doi:10.1126/science.261.5118.201.

Oglesby, D.D., Archuleta, R.J., and Nielsen, S.B., 1998, Earthquakes on dipping faults: The effects of broken symmetry: Science, v. 280, p. 1055–1059, doi:10.1126/science.280.5366.1055.

Oglesby, D.D., Archuleta, R.J., and Nielsen, S.B., 2000, The three-dimensional dynamics of dipping faults: Seismological Society of America Bulletin, v. 90, p. 616–628, doi:10.1785/0119990113.

Oskin, M., and Stock, J., 2003, Cenozoic volcanism and tectonics of the continental margins of the Upper Delfín basin, northeastern Baja California and western Sonora: Geological Society of America Bulletin, v. 115, p. 1173–1190, doi:10.1130/B25154.1.

Oskin, M., Perg, L., Shelef, E., Strane, M., Gurney, E., Singer, B., and Zhang, X., 2008, Elevated shear zone loading rate during an earthquake cluster in eastern California: Geology, v. 36, p. 507–510, doi:10.1130/G24814A.1.

Oskin, M.E., Arrowsmith, J.R., Corona, A.H., Elliott, A.J., Fletcher, J.M., Fielding, E.J., Gold, P.O., Garcia, J.J.G., Hudnut, K.W., Liu-Zeng, J., and Teran, O.J., 2012, Near-field deformation from the El Mayor–Cucapah earthquake revealed by differential LIDAR: Science, v. 335, no. 6069, p. 702–705, doi:10.1126/science.1213778.

Penick, J.L., 1976, The New Madrid earthquakes of 1811–12: Columbia, University of Missouri Press, 155 p.

Philibosian, B., Fumal, T., and Weldon, R., 2011, San Andreas fault earthquake chronology and Lake Cahuilla history at Coachella, California: Seismological Society of America Bulletin, v. 101, p. 13–38, doi:10.1785/0120100050.

Ramirez-Ramos, E.E., 2013, Modelo de estructura de velocidades de corteza para el Sur del Valle de Mexicali, Baja California, México [M.S. thesis]: Ensenada, Baja California, Centro de Investigacion Cientifica y de Educacion Superior de Ensenada (CICESE), 100 p.

Reches, Z., 1983, Faulting of rocks in three-dimensional strain fields: II. Theoretical analysis: Tectonophysics, v. 95, p. 133–156, doi:10.1016/0040-1951(83)90264-0.

Rockwell, T.K., Lindvall, S., Herzberg, M., Murbach, D., Dawson, T., and Berger, G., 2000, Paleoseismology of the Johnson Valley, Kickapoo, and Homestead Valley faults: Clustering of earthquakes in the eastern California shear zone: Seismological Society of America Bulletin, v. 90, p. 1200–1236, doi:10.1785/0119990023.

Rockwell, T.K., Fletcher, J.M., Teran, O., and Mueller, K.J., 2010, The surface rupture of the 2010 El Mayor–Cucapah earthquake and its interaction with the 1892 Laguna Salada rupture—Complex fault interaction in an oblique rift system: American Geophysical Union, Fall Meeting, abs. T51E–01.

Rymer, M.J., and 14 others, 2011, Triggered surface slips in southern California associated with the 2010 El Mayor–Cucapah, Baja California, Mexico, earthquake: U.S. Geological Survey Open-File Report 2010–133, 62 p.

Savage, J.C., Lisowski, M.E., King, N.E., and Gross, W.K., 1994, Strain accumulation along the Laguna Salada fault, Baja California, Mexico: Journal of Geophysical Research, v. 99, p. 18109–18116, doi:10.1029/94JB01471.

Sharp, R.V., and 14 others, 1982, Surface faulting in the central Imperial Valley, *in* The Imperial Valley, California, earthquake of October 15, 1979: U.S. Geological Survey Professional Paper 1254, p. 119–143.

Springer, A., 2010, Constraining the geometry and kinematics on the Santo Tomas segment of the Agua Blanca fault through a combined geophysical and structural study [M.S. thesis]: Tampa, University of South Florida, 58 p.

Suarez, F., Sieh, K.E., and Elders, W.E., 1982, A review of geological effects and damage distribution of the June 9, 1980, Mexicali Valley earthquake, *in* Anderson, J.G., and Simons, R.S., eds., The Mexicali Valley earthquake of 9 June 9, 1980: Newsletter of the Earthquake Engineering Research Institute, v. 16, no. 3, p. 99–105.

Suarez-Vidal, F., Munguía-Orozco, L., González-Escobar, M., González-García, J., and Glowacka, E., 2007, Surface rupture of the Morelia fault near the Cerro Prieto geothermal field, Mexicali, Baja California, Mexico, during the Mw 5.4 earthquake of 24 May 2006: Seismological Research Letters, v. 78, p. 394–399, doi:10.1785/gssrl.78.3.394.

Sykes, L.R., and Seeber, L., 1985, Great earthquakes and great asperities, San Andreas fault, southern California: Geology, v. 13, p. 835–838, doi:10.1130/0091-7613(1985)13<835:GEAGAS>2.0.CO;2.

Townend, J., and Zoback, M.D., 2004, Regional tectonic stress near the San Andreas fault in central and southern California: Geophysical Research Letters, v. 31, no. 15, L15S11, doi:10.1029/2003GL018918.

Unruh, J.R., and Lettis, W.R., 1998, Kinematics of transpressional deformation in the eastern San Francisco Bay region, California: Geology, v. 26, p. 19–22, doi:10.1130/0091-7613(1998)026<0019:KOTDIT>2.3.CO;2.

U.S. Geological Survey, 2006, Quaternary fault and fold database for the United States: http://earthquake.usgs.gov/regional/qfaults/.

Wei, M., Sandwell, D., Fialko, Y., and Bilham, R., 2011, Slip on faults in the Imperial Valley triggered by the 4 April 2010 Mw 7.2 El Mayor–Cucapah earthquake revealed by InSAR: Geophysical Research Letters, v. 38, no. 1, doi:10.1029/2010GL045235.

Wei, S., Fielding, E., Leprince, S., Sladen, A., Avouac, J.-P., Helmberger, D., Hauksson, E., Chu, R., Simons, M., and Hudnut, K., 2011, Superficial simplicity of the 2010 El Mayor–Cucapah earthquake of Baja California in Mexico: Nature Geoscience, v. 4, no. 9, p. 615–618, doi:10.1038/ngeo1213.

Wernicke, B., and Snow, J.K., 1998, Cenozoic tectonism in the central Basin and Range: Motion of the Sierran–Great Valley block: International Geology Review, v. 40, p. 403–410, doi:10.1080/00206819809465217.

Wetmore, P.W., Malservisis, R., Wilson, J., Ferwerda, B., and Alsleben, H., 2012, Kinematics of displacement on the central and western Agua Blanca and Santo Tomas faults, Baja California, Mexico: Seismological Society of America Abstracts with Programs, v. 83, no. 2, p. 373.

Yang, W., and Hauksson, E., 2013, The tectonic crustal stress field and style of faulting along the Pacific North America plate boundary in southern California: Geophysical Journal International, v. 194, no. 1, p. 100–117, doi:10.1093/gji/ggt113.

Yin, Z.-M., and Ranalli, G., 1992, Critical stress difference, fault orientation and slip direction in anisotropic rocks under non-Andersonian stress systems: Journal of Structural Geology, v. 14, p. 237–244, doi:10.1016/0191-8141(92)90060-A.